Using the Rockfall Activity Index to assess the impact of scaling on rock fall activity at Glitter Gulch, Alaska

Kristen Marohl

A report prepared in partial fulfillment of
the requirements for the degree of

Master of Science
Earth and Space Sciences: Applied Geosciences

University of Washington

May, 2019

Project mentor:
Joseph Wartman, UW Civil & Environmental Engineering

Reading committee:
Juliet Crider
Kathy Troost

MESSAGe Technical Report Number: 079

TABLE OF CONTENTS

ACKNOWLEDGEMENTS

The research involved a team of individuals that each contributed an integral piece of data or assistance. I'd like to thank each of the individuals cited in this paper that contributed to the level of understanding I currently have on the topic as well as the professors in the Earth and Space Sciences Department of the University of Washington that honed my knowledge as an adept Urban Geoscientist. I'd like to thank Professor George Bergantz for his furious passion for Engineering Geology that set the tinder for this project. I'd also like to thank Professor Joseph Wartman, Professor Michael Olsen, Shane Markus, and Jake Dafni for their contribution of assistance with data gathering and reduction. Finally, I'd like to thank Professor Juliet Crider and Kathy Troost for their generous guidance and contribution to this report as well as to my continued growth as a geologist.

There are also individuals that I would like to thank that were influential in leading me to this career path. From Kathy Hillig, my High School Advisor who always believed that I could reach any goal I set for myself, and fought earnestly to give me every opportunity possible; to Barbara Clinton, my Community College Honors professor who taught me that I can be inspirational when she wrote of how I opened her eyes to the bias she held against a teenage, single mother, in my letter of recommendation to the University of Washington. From Professor Woody Moses whose passion for Earth and the environment redirected my college career to my passion for geology; to Professor Igor Glozman who pushed my thinking about science and showed me how to be the best geek I can be.

The road that lead to submitting this paper as the final piece of my college target took a village and in no way would I be here today without any one of the following people: Jennifer O'Brien, Megan Dooley, Leslie Hargraves, Michelle Dosey, Keisha Gange, Kurt Marohl, Robyn Gilley, Margaret Reiners, and Blake Furfaro. Thank you all for the special place you have in my life, I appreciate you more than words could express.

I would be remiss to not to thank my MESSAGe Cohort 6 (MC6) team because it wouldn't have been the same without a single one of you wierdos! Mary Alice Benson, Chelsea Ebenezer Bush, Eric Dunham, Ethan Guzek, Hannah Karlsson, Devin Maloney, Austin Rains, Nancy Sackman, Morgan Simon, Aleks Srebro, and Varqa Tavangar... Thank You!

INTRODUCTION

Tens of millions of dollars are spent annually by state transportation departments in the U.S. to protect and maintain roads that intersect geologically unstable slopes (Pierson and Turner, 2012). This money is allocated to not only protect traveling citizens, but to ensure reliable transportation routes for industry, and to safeguard investment in the infrastructure itself. Today, many factors including the environment, rock or soil quality and properties, hydraulic conditions, and construction plans are considered when building roads, with cost efficient longevity of the asset considered (Stead and Wolter, 2015). Historically however, the future effect of the action on a slope was not necessarily considered, and the location of the roadway and the excavation methods used may have been less than ideal (Basahel and Mitri, 2017). The "fast and furious" pace of past construction left many transportation corridors vulnerable to geologically driven hazards and in need of defense (Pierson, 2012).

The most common methods of safeguarding against slope failure fall into two basic categories: stabilization action on the slope, or passive protection of the roadway (Pierson and Vierling, 2012). For a soil-mantled slope, the action approach involves keeping the slope below its angle of repose as determined by its factor of safety and the protection approach involves using retaining structures to hold back the fallen, loose material that is beyond the angle of repose (Wyllie, 2017). Similarly, rock-dominated slopes can be actively maintained through controlled removal of loose material by blasting or mechanical excavation as well as by anchoring loose material with bolts and/or a concrete coating, and the roads can be passively protected by installing ditches and creating barriers or using metal mesh to catch and keep falling rock near the slope (Andrew and Pierson, 2012).

Though the choice for a rock-dominated slope is often stabilization by further excavation, usually by scaling and/or trim blasting, as this appears to be the most economical and least intensive option, it is a temporary fix (2-10 years) that requires continued, if not increased removal (Andrew and Pierson, 2012; Pierson and Vierling, 2012). Scaling is a procedure that involves removal of the "scales" or weathering rind of the rock face, i.e. the loose rock that is predicted to fall in the near future; by its nature, weathering will begin working on the fresh rock and the process will need to be repeated (Andrew and Pierson, 2012). Scaling may be completed by workers suspended on ropes using pry bars, expansive concrete products, and/or air bags, or by heavy machinery such as hydraulic hammers, excavators, and bobcats; strategic blasting may also be used (Andrew and Pierson, 2012; Pierson and Vierling, 2012). Removal of rock on a slope may lead to unplanned increases in rock fall due to destabilization of the slope, over-break on discontinuities or due to elastic rebound, as well as by stress relaxation (Andrew and Pierson, 2012; Wyllie, 2017). In order to properly address each of the hazardous slopes within a transportation agency's domain, efficiency in slope monitoring and maintenance must be increased while maintaining or improving the safety of the field crew (Gigli et al., 2014; Pierson and Turner, 2012; Wyllie 2017).

Historically, it was thought that a thorough site assessment would facilitate a more streamlined maintenance protocol, as site assessments enable the geologist or engineer to understand the processes that lead to failure at a given location empirically (Lato et al., 2012; Basahel and Mitri 2017; Pierson and Turner, 2012). While this is accurate, an agency that has thousands of slopes

intersecting hundreds of assets must have criteria for discerning the relative urgency of attention to a site; the use of a classification scheme can resolve that issue (Pierson, 2012; Pierson and Turner, 2012; Wyllie, 2017). Classification schemes such as the Rockfall Hazard Rating System (RHRS) serve as an efficient communication tool between field staff and designers, as well as facilitating a more judicial evaluation of the rock mass properties and hazards, even when the geology varies (Pierson, 2012).

Unfortunately, classification systems are not without their flaws. The heterogeneous and anisotropic nature of a rock mass means that classification systems can be susceptible to varying interpretations which are biased by the assessor and can be dangerous or impossible to obtain on very high or active slopes (Lato et al., 2012; Gigli et al., 2014; Kromer et al., 2015). Due to budgetary responsibilities, a site is often visited only once, with documentation in the form of field sketches and site photos from ground level (Wyllie, 2017). Some agencies use a drone, but this requires submission of flight plans in advance and post-field assessments are open to communication issues (Pierson, 2012). Additionally, most hazard rating systems don't consider the potential external triggers (Basahel and Mitri, 2017) or identify the potential failure locations on the slope (Kromer et al., 2015).

To correct for the issues mentioned above of subjectivity, access, and the possibility of further assessment after leaving the field, many researchers (e.g. Gigli et al., 2014; Lato et al., 2012) have attempted to improve methodologies for obtaining discontinuity information and rock block size from terrestrial LiDAR scans (TLS), and most commercial software for processing TLS point cloud outputs is set up to aid in the identification of these features (Kromer et al., 2015). These technological advancements have enabled the determination of potential rock fall trajectories and provided the ability to map and quantify rock falls with successive scans over time (Kromer et al., 2015; Gigli et al., 2015; Lato et al., 2012; Stead and Wolter, 2015). Additionally, Matasci et al. (2018) used TLS processing software to create a slope susceptibility index of specific failure mechanisms based on morphology, discontinuity assessments, and long-term monitoring. A main weakness of this line of research however, is that discontinuity surveys do not provide reliable information on slopes comprising poor quality rock or complex and varying morphology (Gigli et al., 2014; Olsen et al., 2015). Recently, a classification scheme called the Rock fall Activity Index (RAI) was developed to address complications in morphology by considering the roughness of the slope in place of mapping the major discontinuities alone (Dunham et al., 2017).

It is assumed that these advancements are effective, but little work has been done to test the level of improvement on efficiency and safety of slope maintenance and monitoring. By identifying likely areas of future failure, can we quantify the effectiveness, in terms of risk depreciation, of rock slope scaling over annual timescales? If we can accurately quantify the effects of scaling, transportation agencies can make maintenance and mitigation decisions more efficiently.

My research examines TLS data on a road cut in the Glitter Gulch area of Alaska, immediately preceding and following a slope stabilization project, noting changes in rock fall and comparing the work done during excavation to the hazardous areas identified through the RAI model. Using the RAI for the study we may also determine its efficacy by noting if the model identified

the same high hazard areas as engineers. In this report, I compare RAI predictions of future failure with on-the-ground assessments of hazard as indicated by scaling activity.

BACKGROUND

Regional Geology

The state of Alaska is largely a syntaxis of accreted terranes. It is identifiable as the bounding of the Gulf of Alaska by the southern reaches of the state that border British Columbia on one flank and the barrier islands to the Bering Sea on the other (Falkowski et al., 2016). The oldest of these, the Precambrian Yukon-Tanana Terrane, is exposed immediately to the north of the continental divide in the Alaska Range (Figure 1). The rocks are metasedimentary oceanic basin rocks and metavolcanics that were first metamorphosed during the Cretaceous collision with the North American Plate and have since experienced localized contact metamorphism via basaltic and granitic intrusion (Falkowski et al., 2016).

Alaska is a geologically active area, with dozens of fault systems (Figure 1) that aid subduction processes in creating active volcanos and large mountains, such as Denali, that have the greatest relief on the North American Continent. Currently, the Pacific Plate and the Yakutat Microplate are subducting in a north-northwest direction, which is translating motion eastward, onto a number of faults including the Chugach, Border Ranges, and Denali faults (Eberhart-Phillips et al., 2006). Near the study site, where a strand of the Denali fault, the east-west trending Hines Creek Fault, intersects the northward draining Tanana River, the basement rocks of the Yukon-Tanana Terrane are exposed on hillslopes and in roadcuts.

Local Geology

The dominant unit of the Yukon-Tanana Terrane is the Birch Creek Schist, a meta-sedimentary schist of marine shale and sandstone origin, whose original structures have been erased during metamorphism. Its greater than 3,000 m thickness is not a true stratigraphic thickness as it is measured perpendicular to the axial plane cleavage (Wahrhaftig, 1968). Wahrhaftig (1968) classified the Birch Creek Schist as mostly quartz with sericite (mica), calcite, and trace albite and microcline (feldspars). Near Denali Park, the Healy Schist, a local sub-unit of the Birch Creek Schist, is a quartz-sericite schist or phyllite with interbedded quartzite that is locally carbonaceous with perfect cubic pyrite up to ¼" in diameter, very fine grained, highly anisotropic, with strong foliation defined by micas (Wahrhaftig and Black, 1958). Near-vertical and irregular joints trend north-south; some have basaltic intrusions (Wahrhaftig and Black, 1958).

Slope failures in the unit have been well documented in studies done for the adjacent railroad; they are typically related to freeze-thaw cycles or high pore-water pressure along foliations; although, some slide planes up to a hundred meters deep have been identified where schist, that has decomposed into clays, retains water in the slope (Wahrhaftig and Black, 1958). This, combined with the high quartzite content of the schist that creates large blocks, can lead to catastrophic failures (Stead and Wolter, 2015). Additional failures can include remobilization of

the loose philitic material that resides on the slope from less severe failures (Stead and Wolter, 2015). Most of this rock fall is evident in the spring when high precipitation on elevated water tables invades weathered regions on slopes and discontinuities that have been jacked open by frost heave are released (Wyllie, 2015).

Study Site

Glitter Gulch is a name given to the area where park concessioners as wells as food and lodging services can be found, just outside the entrance to Denali National Park in the Nenana River Valley, near Healy in the Alaska Range (Figure 2). Located along the George Parks Highway (AK-3), from milepost 239 to 241, is a particularly unstable stretch of rock slopes. Originally constructed in 1971 on cut and filled glacial debris (Wahrhaftig and Black, 1958), this stretch of the highway is reported to have had over 300,000 yd^3 of debris removed by 2008 which included slabs up to 1,000 tons (Cole, 2016). As the main route between Anchorage and Fairbanks in addition to serving all tourists to Denali National Park, the Alaska Department of Transportation and Facilities Services (ADOT&FS) staffs four or more full-time road maintenance personal for mileposts 231-276 alone (Jeff Curry, personal communication, 2018). The slope considered in my study is the near-vertical ~245 m wide and ~30 m tall outcrop immediately north of Fox Creek near milepost 241, within Glitter Gulch (Figure 3).

In 2016, ADOT&FS began a year-long scaling project at Glitter Gulch. The work was prompted when an engineer identified a larger than acceptable risk of rock fall during construction activities for a re-grading project from Mile Posts (MP) 239-252 (Jeff Curry, personal communication, 2018). A scaling crew, Landslide Technology, was hired to remove loose material from the five most hazardous of the eleven slopes along the stretch to be re-graded, by scaling and trim blasting as well as installing extensive barriers between the catchment ditches and the George Parks Highway where the ditch was determined to be insufficient to protect the roadway. The change orders delineating the extent of the ~$15 Million slope maintenance project is attached as an appendix, and a map of the planned work for the slope in my study is shown on Figure 4.

Since 2012, a group known as The Pacific Northwest Transportation Consortium (PacTrans), a multi-University research consortium with the objective of resolving transportation efficiency issues in our region, has been gathering annual terrestrial LiDAR scans of particularly active slopes in Alaska and Oregon, to better understand rock fall activity. A few of their studied slopes in Alaska overlap with the afore-mentioned maintenance project. In my report, I use six years of annual PacTrans terrestrial LiDAR of my study slope: four annual scans prior to scaling, and two following scaling. This provides for three pre-scaling slope activity estimates and one post-scaling rock fall rate on the slope in my study.

The Rockfall Activity Index

One of the recent outputs of PacTrans has been the Rockfall Activity Index (RAI) model, which attempts to make rock slope classifications and monitoring more efficient through the use of photogrammetry and terrestrial lidar scanning with computer modeling (Dunham et al., 2017). It is particularly useful on slopes that are otherwise inaccessible due to height, slope, or heavy rock

fall activity or have rock that is poor quality and highly discontinuous. The RAI uses a high-resolution, 3-D point cloud from terrestrial LiDAR to classify the hazard potential of rock slopes based on their morphology.

The RAI model has already been adopted by the Oregon Department of Transportation to aid their slope assessments and the Alaska Department of Transportation has been using the model less formally (Michael Olsen, personal communication, 2018). These agencies are using the hazard prediction capabilities along with difference analysis of annual TLS data to hone in on areas of high rock fall activity so that passive protection methods may be precisely installed on rock slopes, saving funding by selective mitigation. Additional information such as future failure prediction can also be obtained by looking at the map outputs of the model, which may be helpful in identifying areas in need of maintenance, such as scaling or installation of mesh or other means of limiting hazards.

RAI Software

The RAI algorithm first creates a 5-cm-spaced mesh as a model of the slope and fills isolated empty cells with data based on that of the nearest neighbors in order to minimize error due to data gaps (Figure 5; Markus, 2018). The model then assigns a rock type or morphological classification to each cell of the mesh based on the roughness, as determined by the distance to adjacent cells. The morphological classifications provide a representation of the various ways that a given section of rock may visually appear as well as the typical failure behavior such as: mass wasting (Discontinuous), disintegration (Intact), catastrophic release (Overhanging), and erosion (Talus) (Figure 6; Dunham et al., 2017).

The RAI algorithm then assigns a value of potential hazard, called the RAI Score, to each cell; the score is constructed by combining a measure of the potential energy of a rock fall event from that cell with the given morphological classification, expressed as the annual cumulative delivery of rock fall kinetic energy (kJ) at the base of a unit length (1-m) slope (Dunham et al., 2017). The authors chose this metric to represent their assessment of the hazard of a rock slope for the strong correlation that is seen between the kinetic energy release and the damage caused by the fall. A sum can then be calculated for a given rock slope face, so that relative damage potentials of rock slope faces in a study area may be compared. The formula for the RAI score is,

$$\sum_{i=1}^{n} \frac{1}{2} m_i v_i^2 r_j \ , \tag{1}$$

where n is the number of cells in the 1-meter section, i is the cell number, and j is the number of different morphological classifications in the 1-meter section (Dunham et al., 2017). The mass (m) is calculated based on the volume of rock that is in the 1-meter section as it extends back to its assumed failure plane; the velocity (v) is calculated based on the free-fall potential as calculated from the height above the toe of the slope (disregarding the potential for bounce and deflection); and instability rate (r) is the fraction of cells in the section that are expected to fail in a given year based on change detection done on successive scans during the study (Dunham et al., 2017).

The morphological classifications and related parameters are represented in Figure 6 (Dunham et al., 2017). Shortly after publication, improvements were made to the base parameters by Markus (2018) based on roughly 20,000 failure events spanning 5 years of data at 4 sites in the south-

central region of Alaska, and these improvements were incorporated into the version of the analysis used for my study.

While the orientation of the discontinuities in the rock are not explicitly represented, Dunham et al. (2017) assert that they are accounted for in the instability rate (r). The related instability rates represented in Figure 6 are expected to be applicable to any variety of rock slopes based on the authors' experience with change detection analysis world-wide (Dunham et al., 2017). They do state the obvious caveat that variances in the instability rate (r) should be expected for slopes that: experience more or less weathering, have a groundwater influence, have specific joint sets that increase or decrease the activity, and other factors; in short, the specific rock type and environment can vary the activity rate (Dunham et al., 2017). Concerns as to applicability as a result of varying instability rates can be resolved by surveying and determining parameter values, based on their methods, for a desired rock slope. However, this would require preliminary change detection using LiDAR or Structure from Motion.

Included in the software that processes the RAI algorithm is a change detection algorithm. Change is identified by comparing geo-referenced successive scans, represented as 5-cm-grid mesh (Olsen et al., 2015). Differences in each cell, orthogonal to the best-fit plane and beyond that of the programmed, significant change threshold, are identified and a grid of failures is created that is used to identify change clusters with their own unique event ID (Olsen et al., 2015). The algorithm runs twice, from left to right and then from top to bottom; this insures that clusters are correctly identified (Olsen et al., 2015). Recent additions to the program include output files that summarize statistical metrics such as the loss (or accumulation) volume and volumes of each RAI class.

METHODS

Study Preparation

To define the bounds of this study, it was first necessary to assemble a thorough history of the 2016 scaling work. Jeff L. Currey, P.E., the Natural Resource Materials Engineer for ADOT&FS gave a through account of the project and provided access to the change orders showing the extent of work that was performed; relevant pages are represented in Appendix 1. The sub-contractor that performed the scaling work was also contacted for the as-built and for additional information on the procedures used. I selected one slope for my study from the five underwent scaling in 2016. The selected slope had a significant quantity of maintenance done relative to the size of the slope. The goal was to enable the best before-and-after comparison of the slope and rock fall activity.

Site Assessment

In addition to collecting data to summarize the overall slope, while in the field I gathered parameters for a rock mass classification and for a RHRS score for the outcrop. Tools used in the field were a hand lens, rock hammer, and inclinometer. Personal protective equipment such as reflective vests, climbing helmets, and radios were used by all members of the team as we

were working along a busy highway, beside an active rock slope. Due to factors such as the size of the slope, the busy highway, and the limited field time, in the office, I used Google Earth and GigaPan images, captured by Dr. Joseph Wartman, to aid in completion of the classifications.

Data Acquisition

In the field, laser scanners were used to capture 3D imagery of the study site. These scanners determine 3D relief by sending electromagnetic pulses toward the object(s) and recording the relative time of return after reflection. The 2012 data set was captured by the consulting firm David Evans and Associates using a TITAN Mobile Laser Scan system. The 2013, 2014, 2015, 2017, and 2018 data sets were captured by Dr. Michael Olsen with the assistance of graduate students from the University of Oregon and the University of Washington (including myself in 2018) using a variety of terrestrial laser scanners and related equipment as represented in Table 1. The procedures used by Dr. Olsen involved setting scan positions, on the shoulder of the opposite side of the highway, approximately 60m apart with the scanner set to capture a field of view of at least 180^{o} horizontally by 100^{o} vertically (+70^{o} to -30^{o} from horizontal), for at least 20 minutes to maximize recording time and point density in the allotted field time (Olsen, personal communication, 2018). The scans were joined by GPS with refinements from the manual alignment of targets that were placed on the slope, pre-scan.

Table 1: Data Acquisition equipment used by Dr. Michael Olsen and his team each year in the study. The 2012 data is excluded as it was captured by David Evans and Associates using a proprietary mobile system involving a TITAN Mobile Laser Scanner.

Year	Scanner	Coloring	GPS
2013	Riegl VZ-400	Nikon D700	Trimble R8 GNSS
2014	Riegl VZ-400	Nikon D700	Trimble R8 GNSS
2015	Riegl VZ-400	Nikon D700	Trimble R8 GNSS
2017	Leica ScanStation P40	In-scanner	Trimble R8 GNSS
2018	Riegl VZ-400	In-scanner	Trimble R8 GNSS

*Survey was not conducted in 2016, due to a significant slope maintenance project where scaling and trim-blasting was done on the slope in conjunction with re-paving of the highway.

Data Preparation

As described by Olsen et al. (2015), each scan was logged individually in the field, which necessitated a preliminary transformation to a common coordinate system. The Alaska State Plane Coordinate System Zone 4, North American Datum 1983 (2011) Epoch 2010.00, Geoid 12A was the chosen system.

I then manually cropped the scans to represent only the slope and cleaned them of noisy data, such as significant vegetation, using Maptek's I-Site Studio software. This was done by manipulating narrow (1-5 m) cross-sections of each scan (in each of the three planes) to enable a polygon to be drawn around only the vegetation whose contained points were then deleted from the data set. Care was taken during this step as it was crucial for difference analysis that the

growth or removal of vegetation not be mistaken for a rock fall or accumulation event. I intentionally left some data identified as vegetation as it was chosen to be an accurate proxy for the slope face at that location, rather than leaving a larger data hole. The software created by Dr. Olsen's team that produces the RAI outputs also includes a ground filtering algorithm for minor vegetation removal (Olsen et al., 2015).

To prepare the data for cloud-to-cloud differencing using the RAI software, I finely registered the successive point clouds jointly to minimize error from misalignment. Following methodologies written by the RAI software creators, the prepared scans were imported to an open source point cloud manipulating program, CloudCompare, and finely registered in change epoch year pairs: 2012-2013, 2013-2014, 2014-2015, 2015-2017, 2017-2018. Before using the Finely Register tool, I manually oriented the clouds as close as possible using the Bounding Box Align tool and the Translate/Rotate tool in an effort to expedite processing time. Keeping to the prescribed methodologies, I then noted the number of points that each cloud contained and chose a random sampling unit of $1/20^{th}$ of the largest of the two clouds for the Finely Register tool; the RMS difference was also lowered to $1.0e^{-7}$ and the option to remove the farthest points was chosen. These jointly-registered clouds were then exported as text files to best facilitate file conversion.

The RAI software accepts files of the .bpd type so for the last step of data preparation, I saved the cleaned scans as .txt files and then used a .txt to .bpd convertor provided by Dr. Olsen.

RAI Software Modeling

The software itself operates by having the program, it's options file, and the .bpd files in the same directory and then dragging and dropping in the .bpd files once the desired parameters have been saved in the options file. For this study, parameters for the hole fill window size, closest neighbors used, roughness window, ground filtering, and significant change threshold were kept at the defaults recommended by Dr. Olsen, as significant research supports these values (Olsen et al., 2015 and Markus, 2018). The only variation was with one of the basic bin designators; it was observed that most of the talus accumulation was near a 42^{o} slope angle so a parameter of 44^{o} was chosen as the threshold for identification as talus vs. rock.

Once completed, the output files were imported into Maptek I-site Studio for visual analysis, but any cloud imaging program, including CloudCompare, may be used. Maptek I-site Studio was used based on its processing speed and function of automated instantaneous saving of all work to a program database. These output files are text files with metrics for each grid such as the RAI classification, RAI score, and 3D position.

OBSERVATIONS

Site Characteristics

The study slope presented as a competent, near-vertical mass of schist protruding from the hillside, necessitating a strong bend in the highway that leads to a slight blind corner for the

northbound traveling traffic (Figure 7). The slope is part of an arcuate hill that is a segment of Mount Healy that was separated by the Nenana River. I estimated the uniaxial compressive strength (UCS) of the rock in the field with blows of a standard rock hammer. The rock has a UCS of weak to very weak (<25 MPa) where schist dominated and strong to extremely strong (>25 MPa) where quartzite veining dominates. Micaceous talus clings to the slope above ledges and oxidization stains approximately 75% of the face. The schistosity is parallel/sub-parallel to the slope and there are a few, widely-spaced, intersecting joints with very high persistence.

The RHRS score is between 190 and 304. The dominant control of the score are the overall height of the slope and the very-high-persistence joints. At the time of the site visit, the minimal rock fall present was well within the ditch. However, visible track marks from heavy machinery indicated that the ditch had recently been cleaned. This made it difficult to classify the typical rock fall behavior. Yet, another of the high-hazard mitigated slopes that was not included in this study, had visible track marks as well as rock fall debris on the roadway so it is possible that sufficient time had passed since the ditch/road cleaning for rock fall to have accumulated.

Data Acquisition and Preparation

During the preparation of the data, significant differences in the metadata emerged (Table 2). Resolution of the scanners as well as differences in the spacing of successive scans and length of each scan lead to varying point cloud densities that may represent the slope with more or less accuracy. Alignment accuracy also varied over each change epoch. Each epoch had a lower RMS error than the preceding epoch leading to more accurate change detection potential.

Table 2: Point cloud statistics for each of the six scans as well as successive cloud alignments.

Survey Year	Final Cloud Density (n points)	Alignment Error (m RMS)
2012	1,771,314	
		0.045
2013	23,091,227	
		0.034
2014	51,332,016	
		0.032
2015	69,689,364	
		0.029
2017	69,311,656	
		0.017
2018	116,969,737	

*Survey was not conducted in 2016, due to a significant slope maintenance project where scaling and trim-blasting was done on the slope in conjunction with re-paving of the highway.

FINDINGS

Hazard Data

2012 RAI Outputs
The RAI maps for 2012 are limited due to relatively low resolution of the sparse point cloud acquired in 2012, especially at higher points in the slope (Figure 8).

The portions of the slope that are mapped represent the morphology well (Figure 8A). The lower third of the slope was nearly sufficiently captured and overhangs along discontinuities are accurately identified. The middle, approximately third of the slope, is less than 15% mapped but significant hazards such as the large wedge on the upper-left are, at least in part, identified. The upper third of the slope is not well represented in the RAI analysis with the exception of small spots on the large knob in the upper-center of the slope.

With the caveat of the poor resolution, hazardous areas such as overhangs and small blocky sections around discontinuities are flagged as being significantly hazardous (orange and red in Figure 8B). Better resolution is needed to analyze further.

2013 RAI Outputs
With a 13-fold increase in point density relative to the 2012 scans (Table 2), the 2013 maps provide better resolution (Figure 9).

The morphology is moderately well identified by the RAI classification scheme in the 2013 map (Figure 9A). Very persistent discontinuities are highlighted by lineations of rock mapped as "Widely-Spaced Discontinuous" (dark blue), though those with less persistence are not highlighted as effectively by the RAI classification. Small ledges are mapped well by the presence of "Talus" (purple) on the face of the slope. "Overhanging" (yellow and red) are well mapped but the extent of the block that is related to the overhang is more difficult to recognize, because the RAI does not automatically map the significant discontinuities flanking the overhang. The RAI algorithm does not flag large protrusions that are present.

Mapped hazards are well highlighted but poorly scored (Figure 9B). Large protrusions high on the slope are only mapped as having a moderate hazard (orange) even though there are unfavorable discontinuities having the potential to create blocks up to 9 m in diameter, over 15 m high on the slope. Small block (<0.5 m) potential failures from atop ledges at the same elevation are given approximately the same kJ rating as the large protrusions.

2014 RAI Outputs
The point cloud density doubled between 2013 and 2014 (Table 2), leading to finer resolution of the slope from the 2014 scans (Figure 10).

Morphology mapping patterns follow the results listed for 2013, with the exception of an increase in overall area and a decrease in the area identified as "Intact" (green in Figure 10A). Data gap areas are much smaller than the previous year and the furthest extent of mapping increased. While the increased area increased the volume of rock identified as "Intact", finer

resolution reclassified some “Intact” areas as “Talus” or as “Discontinuous” (blues) and reclassified some “Widely-Spaced Discontinuous” as “Closely-Spaced Discontinuous” (medium blue) and “Fragmented Discontinuous” (light blue). Rock classified as “Overhanging” did not appear to have a significant volume change.

Mapped hazards also gained significant resolution from the previous year (Figure 10B). The color re-distribution from 2013 to 2014 suggests that the total RAI score for the slope likely did not increase though a larger portion of the slope is identified as at least a small hazard. Reclassifications from “Intact” to “Widely-Spaced Discontinuous” increased in hazard while reclassifications from “Widely-Spaced Discontinuous” to “Closely-Spaced Discontinuous” or “Fragmented Discontinuous” decreased hazard.

2015 RAI Outputs

With a 35% increase in point cloud density from 2014 (Table 2), the pattern of year-to-year increases in resolution of the slope maps continued (Figure 11).

The morphology and hazard mapping patterns follow those listed for 2013 and 2014. Due to an increase in resolution, volumes of rock classified as “Intact” decreased while “Discontinuous” and “Talus” classified rock volumes increased (Figure 11A). Additionally, more of the slope is mapped as having some hazard while areas mapped as significant hazard have been further segmented into smaller areas of significant hazard surrounded by lower hazard or no hazard (Figure 11B).

2017 RAI Outputs

Point cloud density remained nearly constant between 2015 and 2017 (Table 2). However, the large maintenance project in 2016 removed significant volumes of rock (predicted to be ~75,000 tons) and reshaped large portions of the slope (Figures 11 and 12).

Morphology identification patterns follow those of 2013 and changes in overall volumes of each morphology type are fairly constant, while local morphology re-classifications between 2015 and 2017 are significant (Figure 12A). The upper left region of the slope where the ~20-meter-wide wedge was removed was re-classified as mostly “Intact” from “Discontinuous” and “Overhanging”, with an underlying ledge of significant “Talus” accumulation (from “Intact”). The upper right region of the slope where the two significant protrusions were minimized and vegetation was removed increased the extent of the mappable area while data holes increased and significant portions of rock classified as “Intact” was re-classified as “Discontinuous” or “Talus”. Over the remainder of the slope, amount of areas classified as “Talus” and “Intact” decreased while “Discontinuous” and “Overhanging” classification areas increased significantly.

The hazard mapping identification patterns follow those indicated in 2013 and 2014 while the patterns of hazard changes follow that of the morphology changes (Figure 12B). The left third of the slope was downgraded significantly in maximum hazard from 2015, but a larger percentage of that section of the slope was re-mapped as having some hazard potential. The remainder of the slope actually increased in overall hazard with many new, small blocks (<0.5 m) being mapped as high hazard (red), and the upper third of the slope nearly doubling in volume mapped as moderate hazard (from zero).

2018 RAI Outputs

The point cloud density nearly doubled from 2015 and 2017 to 2018; yielding four times the number of points of 2013 (Table 2). The useful resolution did not appear to be significantly improved from 2015 and 2017 however (Figure 13).

Morphology identification patterns continue to follow those of 2013. (Figure 13A). The only notable changes in the morphology map are the sizes of data holes, some have increased while others have decreased. Also, the surface area of rock classified as "Talus" downslope of the large wedge removed in 2016 has increased while the area classified as "Intact" decreased.

The overall hazard as indicated by the RAI score appears to have remained fairly constant as well (Figure 13B). The only notable changes are an increase in rock mapped as moderate hazard near the knob at the upper-middle region of the slope.

Change Data

Table 3: Annual rock fall activity data for the slope near MP 241 on the George Parks Highway in Denali, AK from 2012 to 2018 as measured with the RAI software (Olsen et al., 2015). Values are net losses in fractions of cells of that classification type, as determined by the change detection algorithm.

	2012-2013	2013-2014	2014-2015	2015-2017*	2017-2018	2012-2018
Total Loss	0.1052	0.1543	0.0633	0.3579	0.0565	0.7311
Unclassified	0.1518	0.1721	0.1252	0.7578	0.1012	1.4081
Talus	0.0286	0.0488	0.0178	0.3772	0.0395	0.5121
Intact	0.0264	0.1422	0.0122	0.3987	0.0279	0.6077
Widely-spaced Discontinuous	0.1407	0.1462	0.0975	0.5082	0.0754	0.9281
Closely-spaced Discontinuous	0.0984	0.1398	0.0724	0.4559	0.0491	0.7858
Fragmented Discontinuous	0.0781	0.1302	0.0598	0.4558	0.0386	0.7328
Steep Overhang	0.1087	0.1963	0.0984	0.9093	0.0381	1.3011
Cantilevered Overhang	0.2086	0.2588	0.0234	-1.000	0.0820	-0.4268

*Survey was not conducted in 2016, due to a significant slope maintenance project where scaling and trim-blasting was done on the slope in conjunction with re-paving of the highway.

Epoch 1: 2012-2013

Even with significant hole filling due to the low resolution from the mobile scanner used to gather the 2012 data, change detection losses suggesting rock fall appear in the expected areas by visual inspection as well as those identified as hazardous by the RAI Score (Figure 14). Loss clusters follow expected areas of rock fall such as along major discontinuities, under overhangs, and in areas of talus accumulation. Each area identified as high hazard or moderate hazard by the RAI Score experienced a loss, at least partially. Significant losses lower in the slope were not predicted by the RAI Score map even though some were as high as 6 m from the base of the slope. Unfortunately, resolution was poorest in critical areas such as the highest points of the slope. Nearly all gains were points that were absent from the 2012 image (due to cropping) or were assigned an Unclassified morphology by the RAI software; the very few actual gains, at the base of the slope, were classified as Talus.

Epoch 2: 2013-2014

Similar to Epoch 1, there are expected areas of loss based on discontinuities and morphology types in the center of the slope, but there is significant loss identified to the left and right reaches on the scan due to a misalignment of the scans (Figure 15). Gains at the upper reaches of the slope align with points that were assigned an "Unclassified" morphology by the RAI software in 2013 and were absent (due to cropping) in 2014; while gains at the base of the slope were classified as "Talus" by the RAI software.

Epoch 3: 2014-2015 Epoch

Losses in this epoch follow the pattern of losses in the previous two; most of the clusters are in locations where there are discontinuities, overhangs, and ledges (Figure 16). The perimeter shows extensive gains and there are patches of gains mainly encircling data holes. These apparent gains do not represent slope processes, but result from slight changes in extent of the data.

Epoch 4: 2015-2017 Epoch

As expected, there were significant losses between these 2015 and 2017 (Figure 17), due to scaling operations on the slope. The large overhanging wedge in the upper left was removed as well overhanging massive section in the upper right. Much of the remaining losses follow lesser overhangs identified as high and moderate hazard, and ledges with significant "Talus" classified. Unexpected were the significant patches of gains appearing sporadically along the upper third of the slope, adjacent to significant losses.

Epoch 5: 2017-2018 Epoch

Though recently scaled, which should have reduced rock fall, significant losses appear around the perimeter of the large wedge that was removed on the upper left section of the slope as well as on the discontinuities below, on the lower left (Figure 18). Small, losses are scattered across the slope face with a slight concentration on the upper third of the slope and along the major

discontinuities, particularly on the lower right side of the slope. There is a region of gains along the right edge of the slope and small patches of gains throughout, but typically where there are data holes.

DISCUSSION

Rock Fall

A significant hurdle in the analysis of rock fall with the RAI model in the study was the inconsistent quality of available data. The point cloud scan from 2012 was incomplete while the 2013 scan and potentially the 2014 did not provide sufficient point density to enable discussions of morphology change across years with better resolution, without significant error due to resolution-driven classification changes. Additionally, limitations of the current RAI software do not allow for meaningful analysis of the metrics produced, such as volumes of morphology type and unique cell identifiers for morphology change assessment, without significant levels of programming ability and processing power.

The rock type of the study slope did not lend itself well to a strong discussion about rock fall and the RAI model. The high strength of much outcrop meant than annual rockfall activity was low. Rockfall was mostly centered around local areas of high weathering such as on small ledges and along discontinuities; most trackable losses were likely talus or individual small blocks. The crystalline nature of the rock did however, provide meaningful insight as to how poorly formed discontinuities on an intact face can begin to be identified by roughness.

Regardless, the overall pattern of rock fall over the 5 change epochs, with concessions for the resolution and misalignment errors, shows some consistency before the scaling and a less than remarkable decrease post-scaling (Table 3). Net annual loss during Epoch 3 (preceding scaling) was 6.33 percent of the slope, while net annual loss Epoch 5 (following scaling) was 5.65 percent of the slope; a change of 0.68 percent. Decreased losses did occur in rock classified as higher hazard such as “Discontinuous” (9.75, 7.24, and 5.98 to 7.54, 4.91, and 3.86) and “Steep Overhang” (9.84 to 3.81), but other classifications increased in losses post-scaling. This indicates that while scaling changes the hazards it may not diminish overall rock fall volumes. The significant amount rock fall activity post scaling could be attributed to the slope attempting to reach a new equilibrium after large removals during maintenance or possibly due to damage caused by the maintenance processes themselves.

Excavation Damage

Due to the lack of a standard methodology for removal of rock, scaling methods are not consistent; also, the type and extent of scaling work completed during the 2016 mitigation project represented here, is unknown. Often, large pry bars and air bags that are used to force rock loose can impart damage on the underlying, fresh rock (Wyllie, 2017; Hook, 2007). In addition to direct damage to the surrounding rock, removal of key pieces that kept others locked in their position can passively damage the slope; the stress state on the remaining block(s) shifts from one of compression to tension and the strength is greatly weakened (Hook, 2007). This is

may be the case for the study slope, as many more overhangs are present post-scaling. This increase can be identified by comparing the amount of yellow and red cells from Figure 11 to Figure 12, particularly in the center and upper-right of the slope.

Data Error

Errors (in the form of misidentification of change) arise due to a variation of the 3-D surface created from the point cloud in subsequent years that are independent of any actual change in the geometry of the slope face. Alignment errors are significantly less than the chosen threshold for change so any error present would be due to resolution or filtering. The most common cause of a misrepresented 3-D surface is vegetation that is incompletely removed being represented as part of the slope face; this may be partially corrected by a hole filling algorithm but may still result in mis-identification of slope failures (see Markus 2018). Hole filling can be significant, even in a very dense and well-cleaned data set (Figure 19).

RAI Hazard

The RAI model, while useful for the quantification of rock fall hazards on a rock slope, enabling slope hazard ranking, fails to identify key risk factors that are incorporated in the more qualitative models that it is attempting to supersede, such as the RHRS. While the RAI model may identify a slope as of the highest hazard, said slope may lie on a road with low traffic and a ditch wide enough to capture most or all of the presumed failures. Additionally, it fails to account for other types of failures such as topples and slides which may be a dominant failure mode for rock slopes with persistent failure planes parallel to the face.

A notable phenomenon is that a surface, visually identifiable as one block or unit, may be delineated as multiple rock types by the RAI software due to a change in the identified surface roughness. While this occurrence may appear to be an error, it can aid in identifying hazard by highlighting potential future failure planes (discontinuities) that are not visible to the naked eye. This also enables the geologically trained eye to pick out large blocks or wedges by noting the outline of such an object, created by the highlighting of rougher areas around the intact object. This could be enhanced by including a means to identify significant relief off of the slope face in the x and y planes in addition to the z-plane.

CONCLUSIONS & RECOMMENDATIONS

Efficacy of Scaling

The low number of change epochs, limited rock type variability, and singular site of this study limits the ability to make global conclusions about the validity of scaling on unstable rock slopes. However, even with allowances for systematic errors which can be easily identified, rock fall activity was reduced by only approximately 1% in the epoch immediately following the extensive maintenance project. The cost of the 2016 scaling project as well as the ongoing costs associated with ditch and road maintenance should not be discounted; the sum of these

continuing expenses may quickly overshadow the cost of a more extensive and long-term stabilization project.

Effectiveness of the RAI

Though my slope has a different rock type than the RAI classification scheme was designed for, morphologies on the slope face were well mapped. The massive, quartzite-rich, phyllite-schist is not considered poor quality in this outcrop and fails differently than a more micaceous outcrop would which would be better suited for the RAI. Regardless, techniques similar to a visual slope classification such as looking for intact portions surrounded by significant relief (overhangs) are able to identify large blocks from the RAI classification outputs. While doing so eliminates some of the intended automation, the RAI classification is still valuable in mapping morphology for hard to see and dangerous slope sections.

According to rock fall activity at this site, from 2012-2018, the RAI score was effective in identifying hazardous areas. For each change epoch, the significant losses on the slope were identified by the RAI score as being of at least moderate hazard. However, significant-sized failures are not scaled accordingly; there should be some metric that clumps potential failures into clusters that could have a higher rating. An issue for further consideration would be that failure planes parallel to the slope face or which daylight infrequently can lead to some of the most catastrophic failures and are not explicitly highlighted by the RAI Score. It would be prudent for emergency and infrastructure managers and planners to use a combination method, the RAI model as well as a thorough geologic assessment, including a discontinuity survey, for complete slope analysis.

Future Work

Future studies on already existing data could make this study more robust. More change epochs that could identify a new rock fall activity state after the relaxation period should be gathered. Data for the same time periods exists for at least two of the other four slopes worked on in this same maintenance project that could be analyzed to confirm the findings of this study. Similarly, comparing with a proximal, non-scaled outcrops over the same years can account for any background changes in rock fall due to climatic or environmental fluctuations.

REFERENCES CITED

Andrew, R.D., and Pierson, L.A., 2012, Stabilization of Rockfall *in* Turner, K.A., Schuster, R. L., eds., Rockfall: Characterization and Control: Washington, D.C., Transportation Research Board, p. 468-492.

Basahel, H., and Mitri, H., 2017, Application of rock mass classification systems to rock slope stability assessment: A case study: Journal of Rock Mechanics and Geotechnical Engineering, v. 9, no. 6, p. 993-1009.

Cole, D., 2016, Rock climbers put their skills to work improving highway safety near Denali Park: https://www.adn.com/business-economy/energy/2016/06/25/denali-climbers-chip-away-at-crumbling-rock-walls-as-summer-traffic-flows-by-100-feet-below/ (accessed August 2018).

Dunham, L., Wartman, J., Olsen, M.J., O'Banion, M.S., and Cunningham, K., 2017, Rockfall Activity Index (RAI): A lidar-derived, morphology-based method for hazard assessment: Engineering Geology, v. 221, p. 184-192.

Eberhart-Phillips, D., Christensen, D., Brocher, T., Hansen, R., Ruppert, N., Haeussler, P., and Abers, G., 2006, Imaging the transition from Aleutian subduction to Yakutat collision in central Alaska, with local earthquakes and active source data: Journal of Geophysical Research: Solid Earth, v. 111, 31p.

Falkowski, S., Enkelmann, E., Drost, K., Pfänder, J.A., Stübner, K., and Ehlers, T.A., 2016, Cooling history of the St. Elias syntaxis, southeast Alaska, revealed by geochronology and thermochronology of cobble-sized glacial detritus: Tectonics, v. 35, p. 447–468.

Gigli, G., Morelli, S., Fornera, S., and Casagli, N., 2014, Terrestrial laser scanner and geomechanical surveys for the rapid evaluation of rock fall susceptibility scenarios: Landslides, v. 11, no. 1, p. 1-14.

Hook, E., 2007, Practical Rock Engineering: https://www.rocscience.com/learning/hoeks-corner/course-notes-books (accessed June 2018).

Kromer, R.A., Hutchinson, D.J., Lato, M.J., Gauthier, D., and Edwards, T., 2015, Identifying rock slope failure precursors using LiDAR for transportation corridor hazard management: Engineering Geology, v. 195, no. 3, p. 93-103.

Lato, M., Diederichs, J., Hutchinson, M., and Harrap, S., 2012, Evaluating roadside rockmasses for rockfall hazards using LiDAR data: Optimizing data collection and processing protocols: Natural Hazards, v. 60, no. 3, p. 831-864.

Markus, S., 2018, Morphological Evolution of Rock-Slopes and Assessing the Rockfall Activity Index (RAI) Methodology: University of Washington, 135 p.

Matasci, B., Stock, G.M., Jaboyedoff, M., Carrea, D., Collins, B.D., Guérin, A., Matasci, G., Ravanel, L., 2018, Assessing rockfall susceptibility in steep and overhanging slopes using three-dimensional analysis of failure mechanisms: Landslides, v. 15, no. 5, p. 859–878.

Olsen, M.J., Wartman, J., Mcalister, M., Mahmoudabadi, H., O'Banion, M.S., Dunham, L., and Cunningham, K., 2015, To Fill or Not to Fill: Sensitivity Analysis of the Influence of Resolution and Hole Filling on Point Cloud Surface Modeling and Individual Rockfall Event Detection: Remote Sensing, v. 7, no. 9, p. 12103-12134.

Pierson, L.A., 2012, Rockfall Hazard Rating Systems *in* Turner, K.A., Schuster, R.L., eds., Rockfall: Characterization and Control: Washington, D.C., Transportation Research Board, p. 56-71.

Pierson, L.A., and Turner, K.A., 2012, Implementation of Rock Slope Management Systems *in* Turner, K.A., Schuster, R.L., eds., Rockfall: Characterization and Control: Washington, D.C., Transportation Research Board, p. 72-110.

Pierson, L.A., and Vierling, M.P., 2012, Mitigation Selection *in* Turner, K.A., Schuster, R.L., eds., Rockfall: Characterization and Control: Washington, D.C., Transportation Research Board, p. 445-456.

Stead, D., and Wolter, A., 2015, A critical review of rock slope failure mechanisms: The importance of structural geology: Journal of Structural Geology, v. 74, p. 1-23.

Wahrhaftig, C., 1968, Schists of the Central Alaska Range: U.S. Geological Survey, Bulletin 1254, 22 p.

Wahrhaftig, C., and Black, R.F., 1958, Quaternary geology of the Nenana River valley and adjacent parts of the Alaska Range; Engineering geology along part of the Alaska Railroad: U.S. Geological Survey, Professional Paper 293, 118 p.

Wilson, F.H., Hults, C.P., Mull, C.G., and Karl, S.M., comps., 2015, Geologic map of Alaska: U.S. Geological Survey Scientific Investigations Map 3340, pamphlet 196 p., 2 sheets, scale 1:1,584,000, http://dx.doi.org/10.3133/sim3340.

Wyllie, D.C., 2015, Rock Fall Engineering: Boca Raton, CRC Press/Taylor & Francis Group, 243p.

Wyllie, D.C., 2017, Rock Slope Engineering: Civil Applications Fifth Edition: Boca Raton, CRC Press/Taylor & Francis Group, 620p.

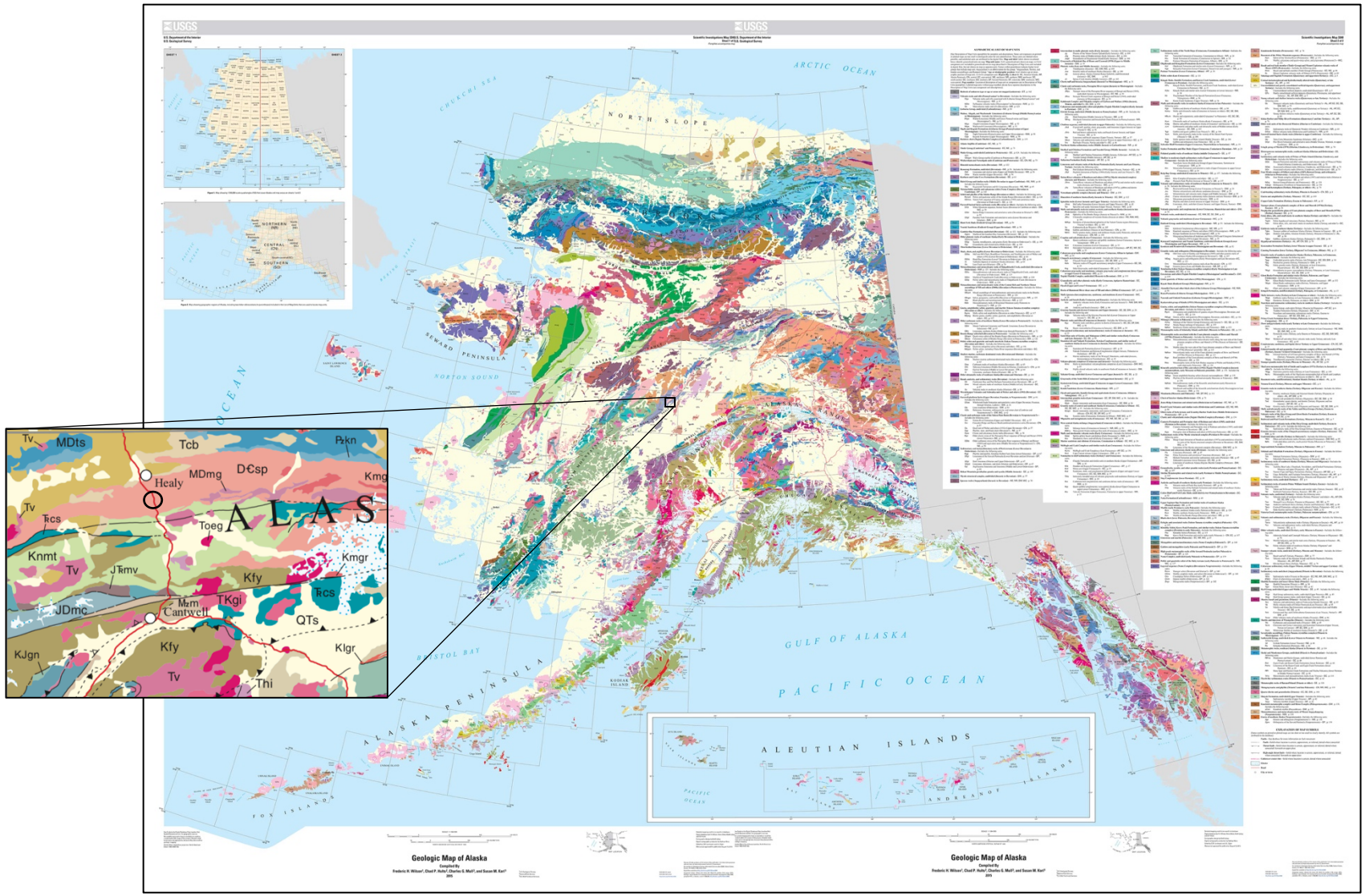

Figure 1: Geologic Map of Alaska with an inset of the 1:250,000 Healy Quadrangle encompassing the study area, circled in black (Wilson et al., 2015). The relevant unit for the study area is D€sp: Pelitic schist and quartzite and mafic interbeds (Yukon-Tenana crystalline complex; Devonian and older).

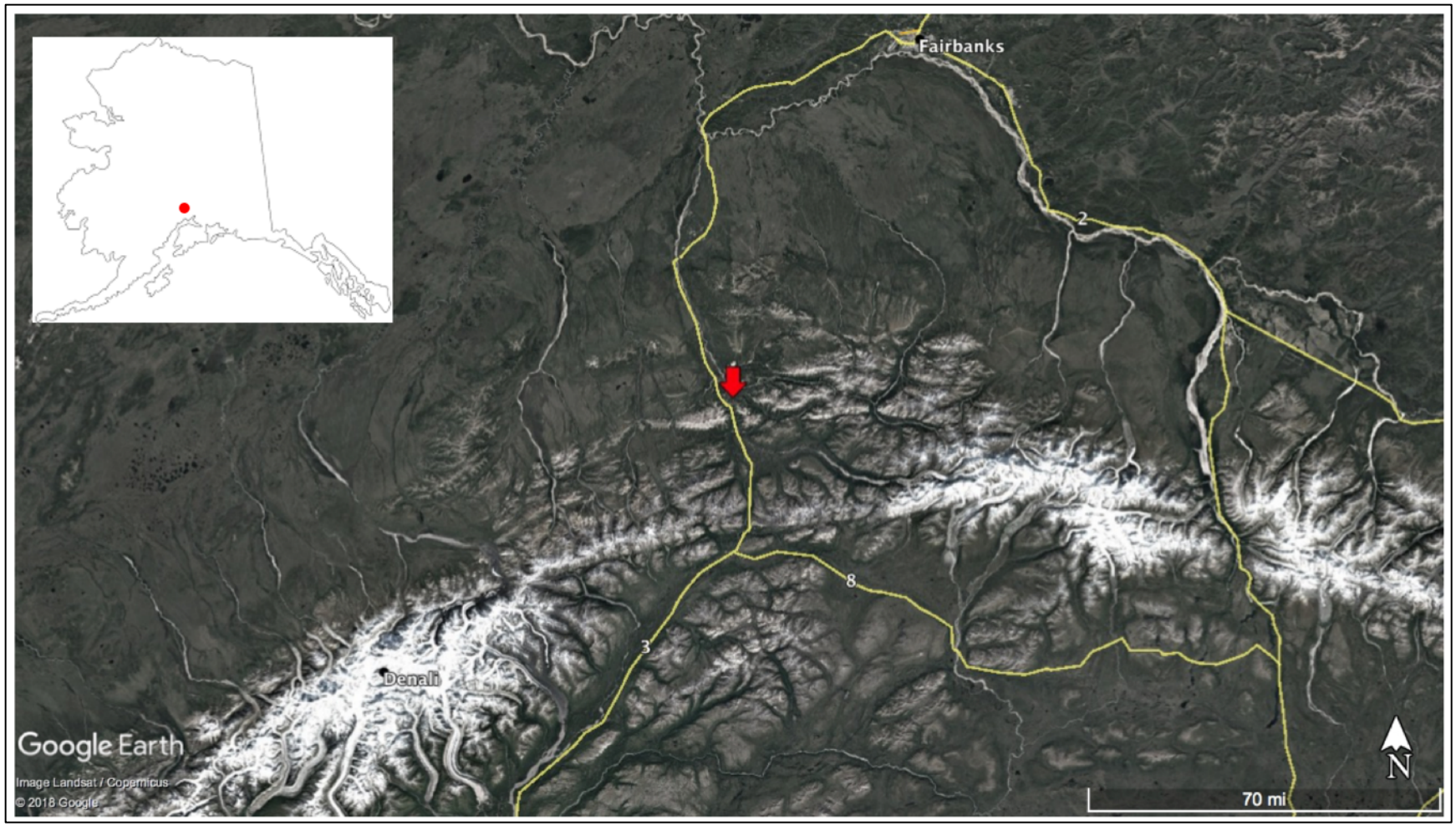

Figure 2: Satellite image and road map obtained from Google Earth of the Glitter Gulch study site outside of Denali National Park in Alaska. State Route 3, also known as Alaska Interstate 3 and more commonly referred to as the George Parks Highway, is the effected transportation route. As well as servicing the park, the highway is the main transportation route between Anchorage and Fairbanks. The inset shows location within the state of Alaska.

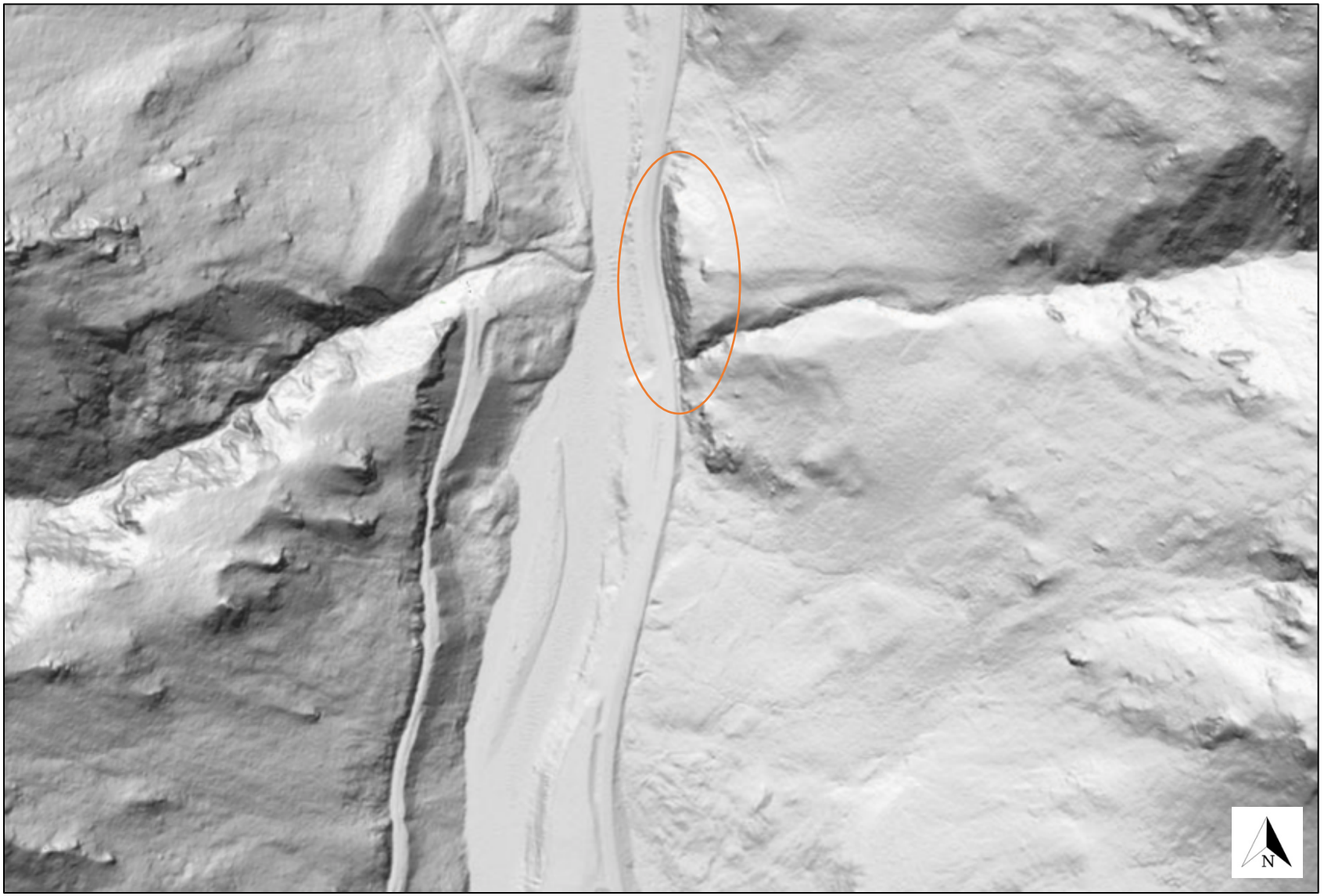

Figure 3: Aerial LiDAR of study area (circled in orange) obtained from the State of Alaska's Department of Geological and Geophysical Surveys on 08/20/18. The long axis of the orange ellipse is approximately 0.3 km. The Nenana River, a tributary to the Tanana River that drains the Northern slopes of Denali, runs north-south through the center of the image and is bordered on the east by Alaska Interstate 3. The Alaska Railroad can be seen cutting the slope west of the river.

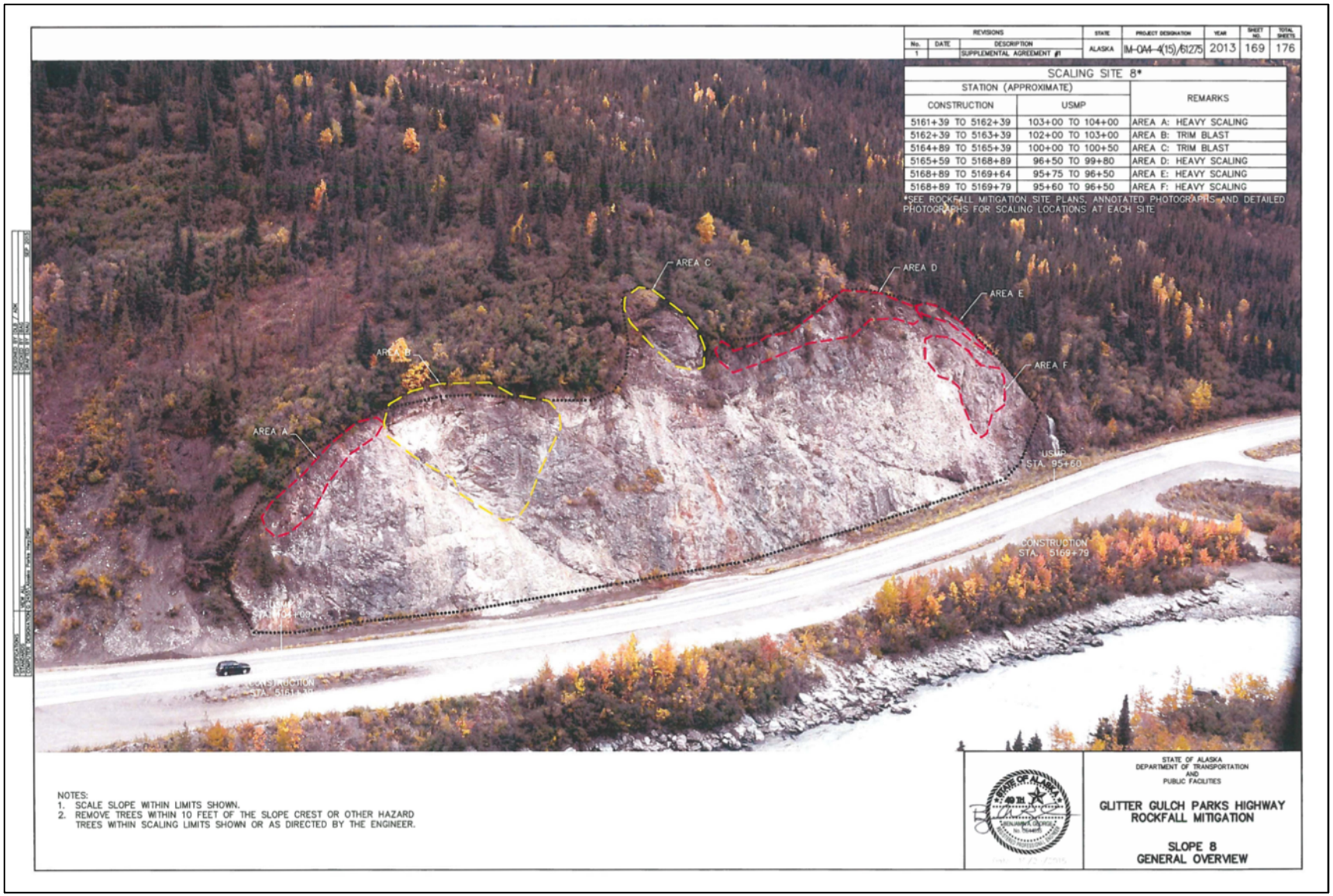

Figure 4: Annotated oblique aerial image of the study outcrop generated by ADOT&FS denoting the planned areas for scaling (red) and trim blasting (yellow) for the 2016 maintenance project.

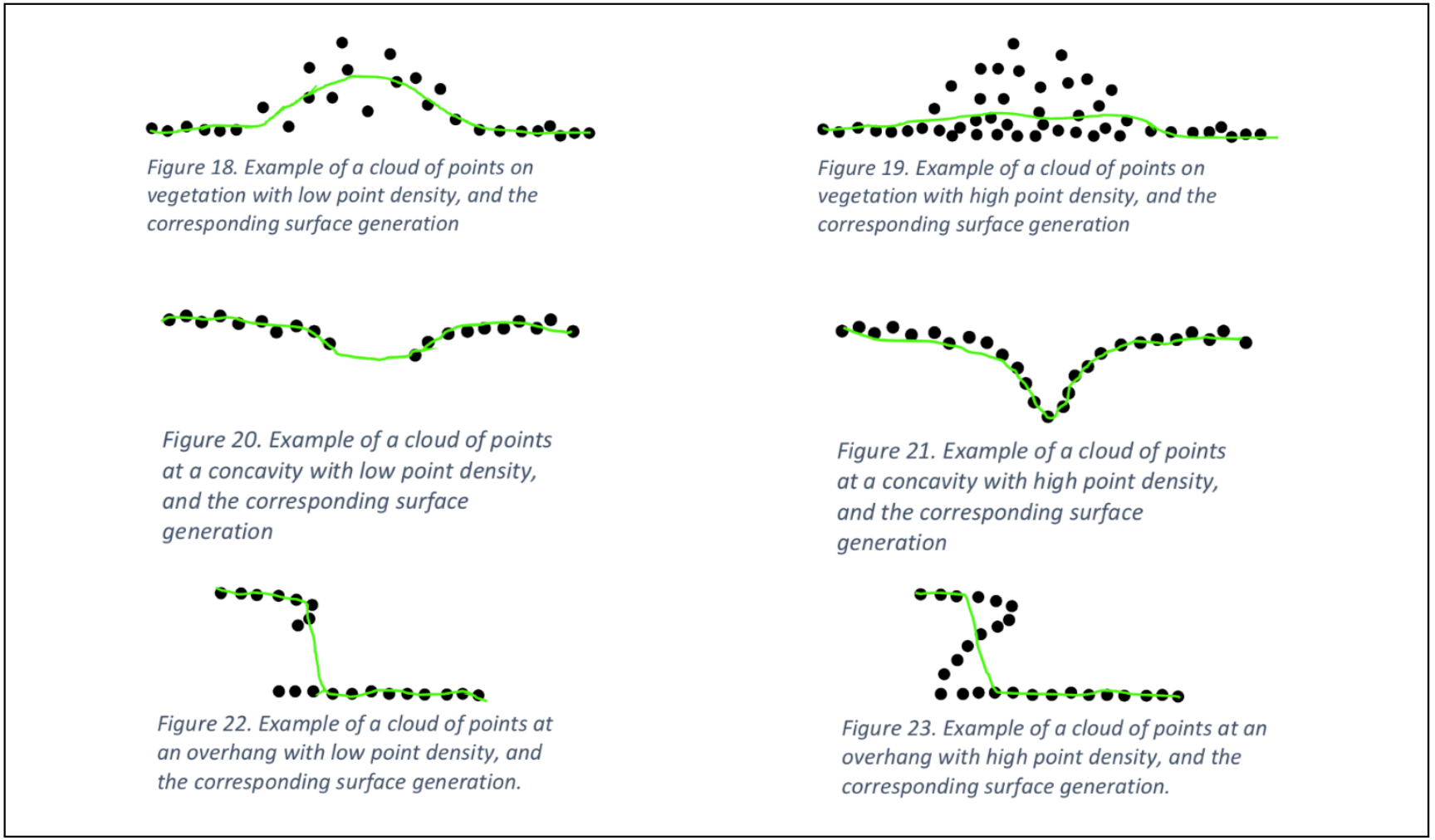

Figure 18. Example of a cloud of points on vegetation with low point density, and the corresponding surface generation

Figure 19. Example of a cloud of points on vegetation with high point density, and the corresponding surface generation

Figure 20. Example of a cloud of points at a concavity with low point density, and the corresponding surface generation

Figure 21. Example of a cloud of points at a concavity with high point density, and the corresponding surface generation

Figure 22. Example of a cloud of points at an overhang with low point density, and the corresponding surface generation.

Figure 23. Example of a cloud of points at an overhang with high point density, and the corresponding surface generation.

Figure 5: Images from Markus (2018) representing the various ways a surface may be represented based on various point cloud densities and point distributions.

RAI method morphological classes and associated failure mass depths and instability rates.

Morphological classification	Description	Estimated depth of failure mass (m)[a]	Instability rate (r) [%][b]	Estimated typical range of instability rate (r) values[c]
Widely to moderately spaced discontinuous rock (D_w)	Intact blocks or fragments of rock separated by discontinuities typically spaced at ~30 cm or greater	0.3	0.71	0.4–3.0
Closely spaced discontinuous rock (D_c)	Intact blocks or fragments of rock separated by discontinuities typically spaced between ~10 cm and ~20 cm	0.2	0.34	0.2–2.0
Fragmented discontinuous rock (D_f)	Intact blocks or fragments of rock separated by discontinuities with a typical spacing of less than ~10 cm	0.1	0.18	0.1–1.0
Intact rock (I)	Rockmass with few or relatively minor discontinuities	0.05	0.1	0.02–0.3
Cantilevered overhang (O_c)	Overhanging rock whose lower portion is inclined at less than 120° [see Fig. 1]	0.5	1.98	1.0–5.0
Steep overhang (O_s)	Overhanging rock whose lower portion is inclined at greater (i.e., steeper) than 120° [see Fig. 1]	0.75	1.97	1.0–5.0
Talus (T)[d]	Mass wasting-derived rock fragments (debris) accumulated at the base of a slope, or along benches within a slope	0.025	0	0–0.4

[a] Estimated depth of the failure mass is based on annual change detection data collected at the field study sites. The resulting failure volume for each 5-cm by 5-cm slope face cell is computed by multiplying the cell area (i.e., 25 cm^2) by the estimated depth of the failure mass.

[b] The instability rate r is computed as the fraction of the cells within a morphologic unit that failed (eroded) based on annual change detection data obtained at the field study sites in Alaska, USA.

[c] The typical range of r values is estimated based on the authors' involvement with change detection studies at rock slope sites worldwide. The values vary based on a variety of factors including rock type, weathering, subsurface characteristics, and environmental conditions with lower bound values correspond to relatively stable conditions while upper bound values slopes that actively produce rockfall. Note that these values are associated with a high degree of variability and uncertainty.

[d] The r value represents erosion and raveling of talus.

Figure 6: Morphological classifications and their values for the RAI model (Dunham et al., 2017).

Figure 7: Aerial photo taken in August 2018, of the study slope at MP 241 on the George Parks Highway near Glitter Gulch, Alaska. The image was captured with a DJI Phantom 4 drone flown by Jake Dafni. North is to the left; Sugar Loaf Mountain is in the distance and the Nenana River is in the foreground. Quartzite dominated regions of the outcrop present as grey while more micaceous regions appear brown in this image.

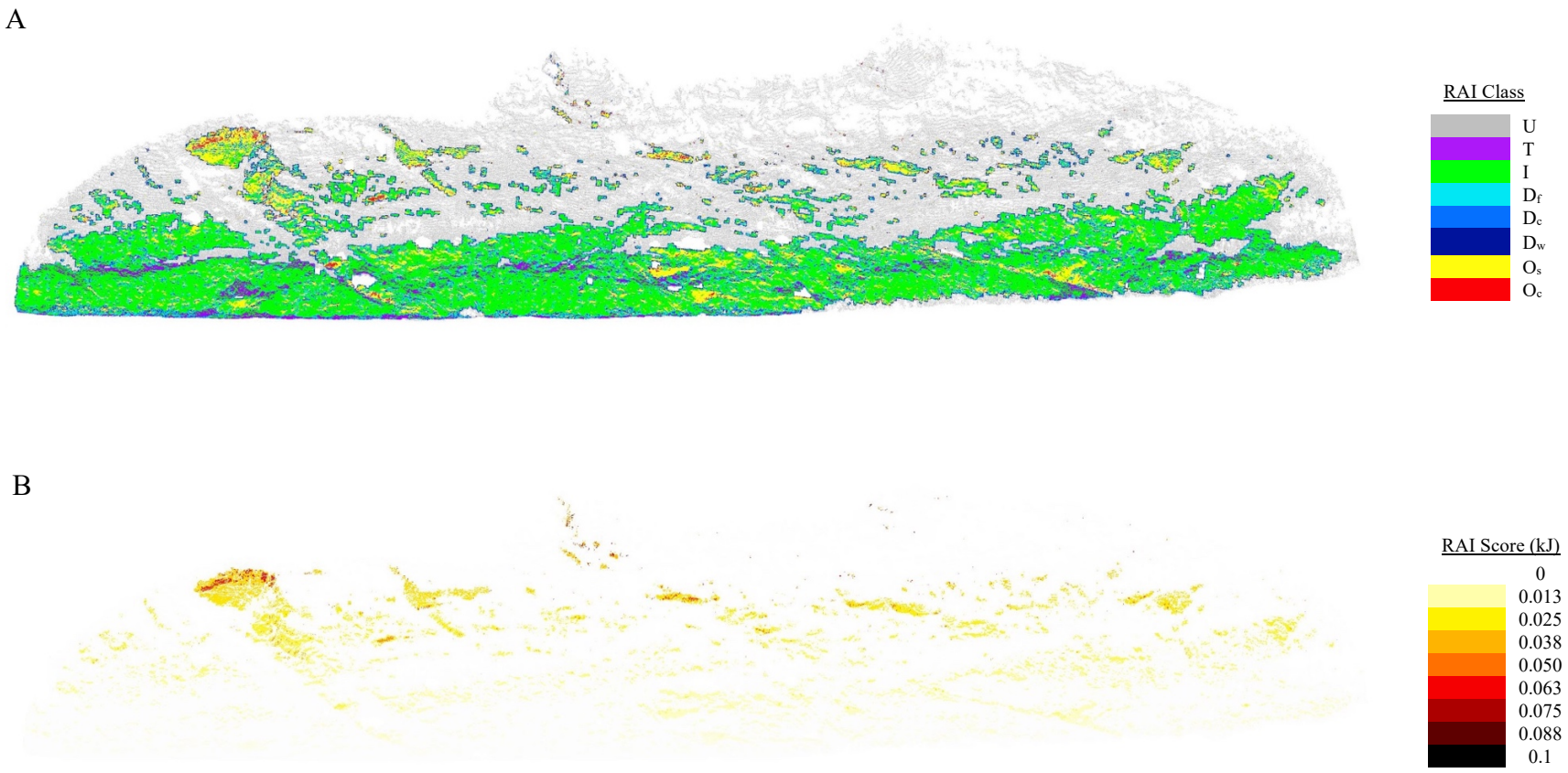

Figure 8: RAI Classes (A) and RAI Scores (B) for the 2012 scan of the study slope at MP 241 on the George Parks Highway near Glitter Gulch, Alaska. Refer to Figure 6 for a description of the RAI Classes. The white areas in A are holes in the data set and grey areas are where there is insufficient data for classification of a morphology type.

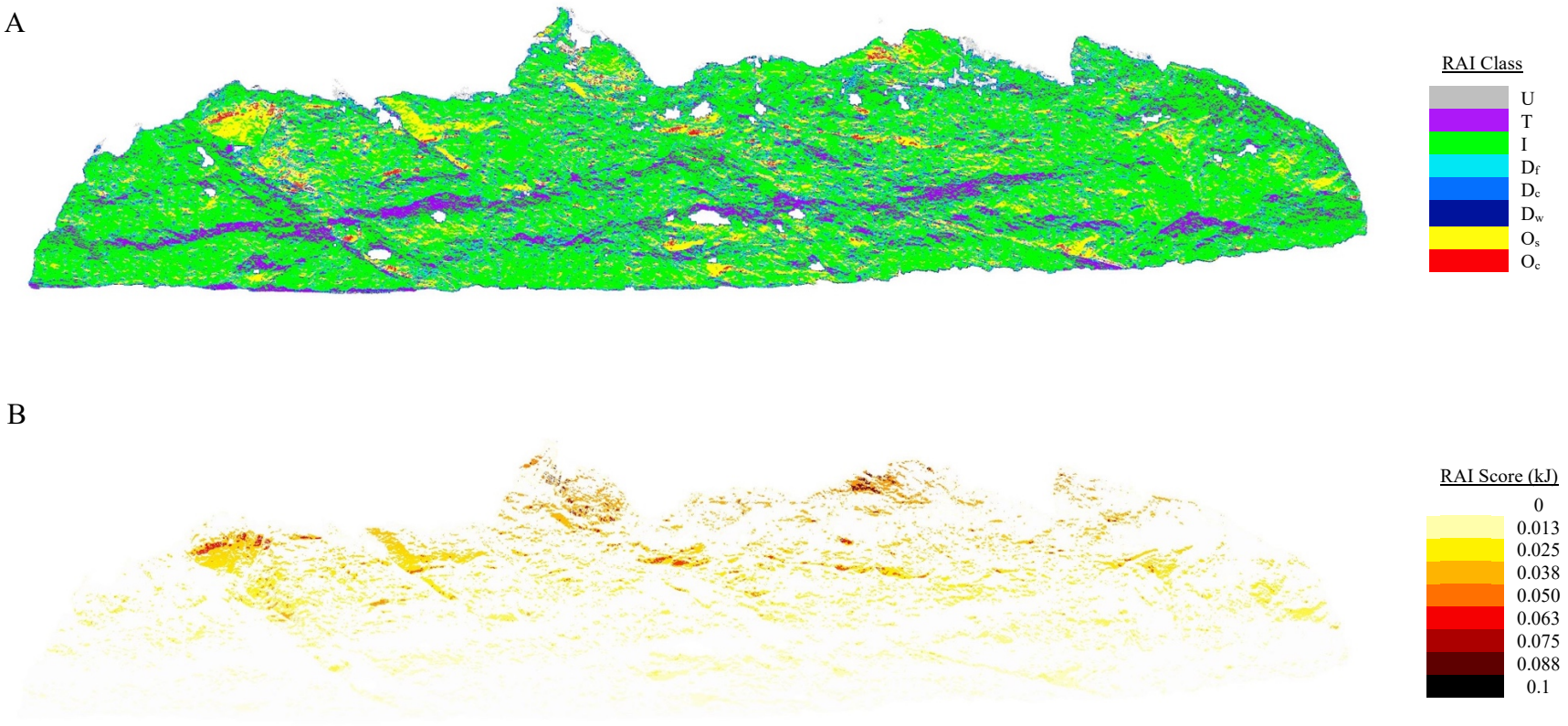

Figure 9: RAI Classes (A) and RAI Scores (B) for the 2013 scan of the study slope at MP 241 on the George Parks Highway near Glitter Gulch, Alaska. Refer to Figure 6 for a description of the RAI Classes.

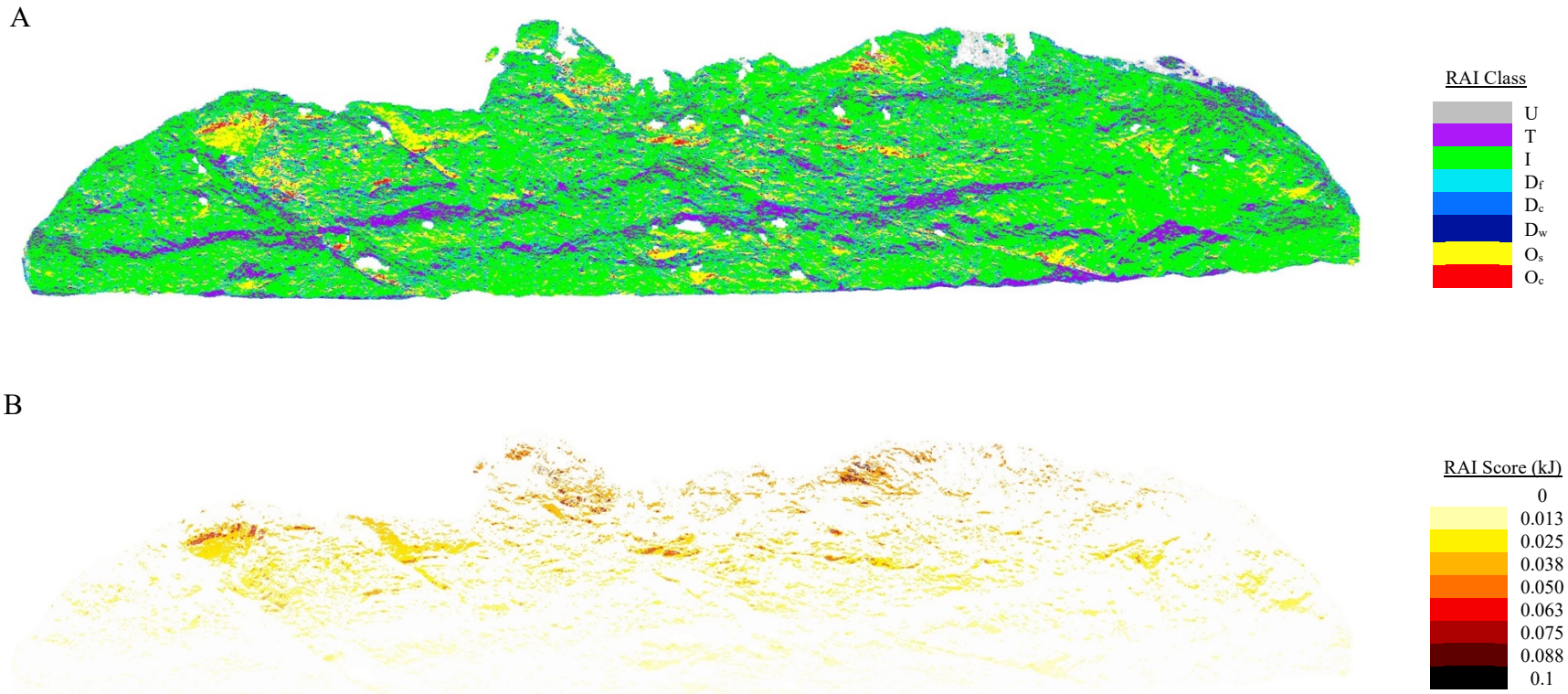

Figure 10: RAI Classes (A) and RAI Scores (B) for the 2014 scan of the study slope at MP 241 on the George Parks Highway near Glitter Gulch, Alaska. Refer to Figure 6 for a description of the RAI Classes.

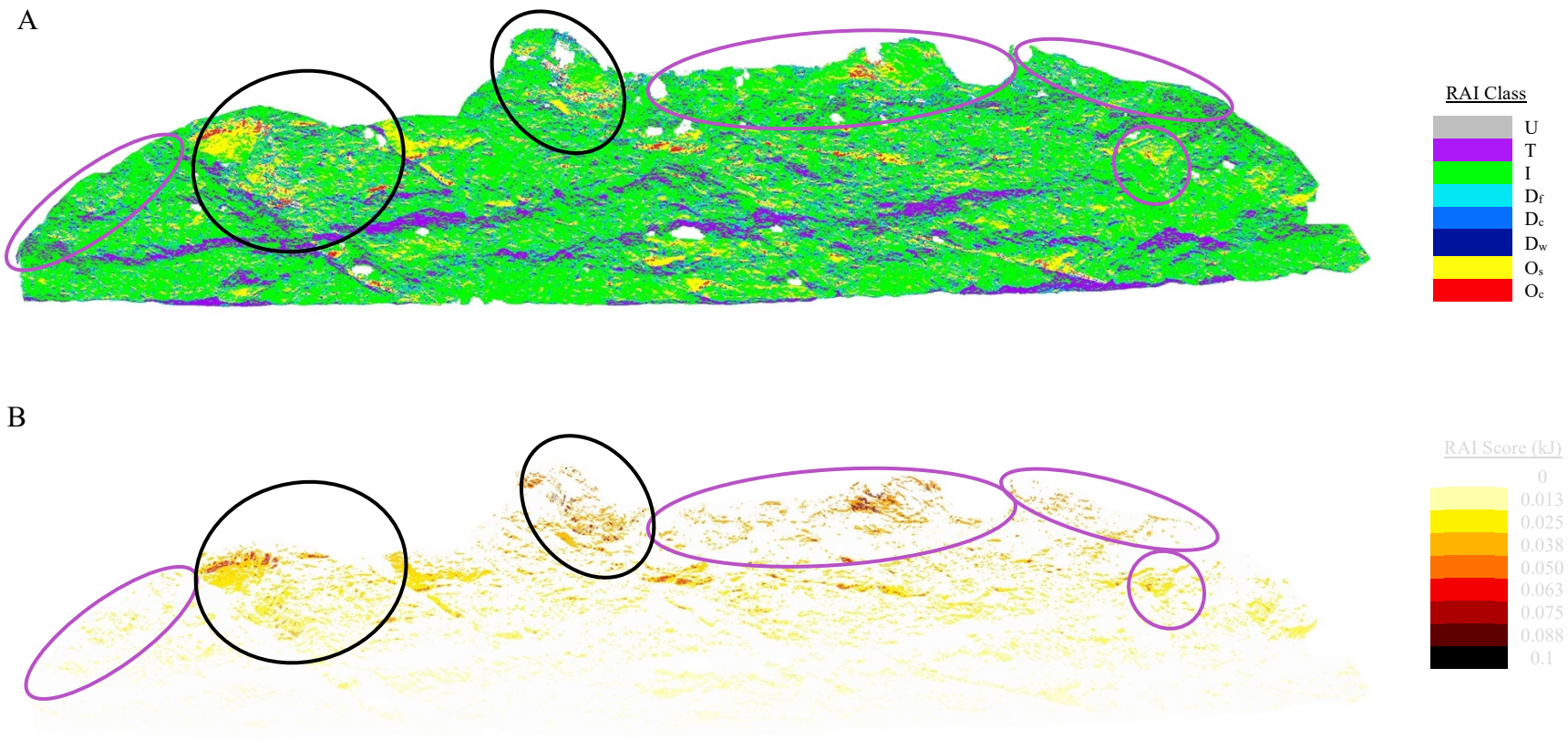

Figure 11: RAI Classes (A) and RAI Scores (B) for the 2015 scan of the study slope at MP 241 on the George Parks Highway near Glitter Gulch, Alaska. Refer to Figure 6 for a description of the RAI Classes. Planned mitigation areas are circled in purple for scaling and black for trim blasting. (Compare to Figure 4.)

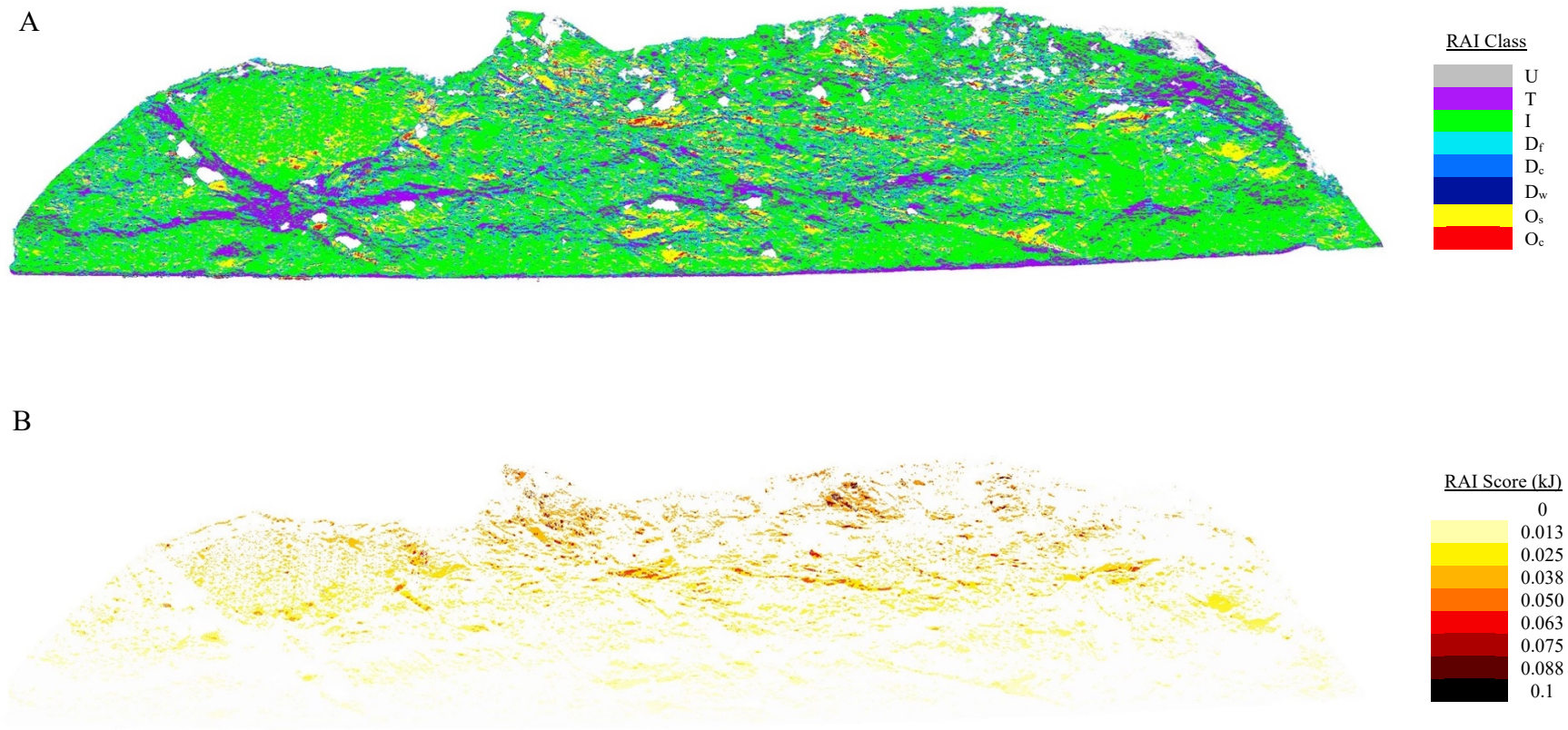

Figure 12: Post-scaling RAI Classes (A) and RAI Scores (B) for the 2017 scan of the study slope at MP 241 on the George Parks Highway near Glitter Gulch, Alaska. Refer to Figure 6 for a description of the RAI Classes.

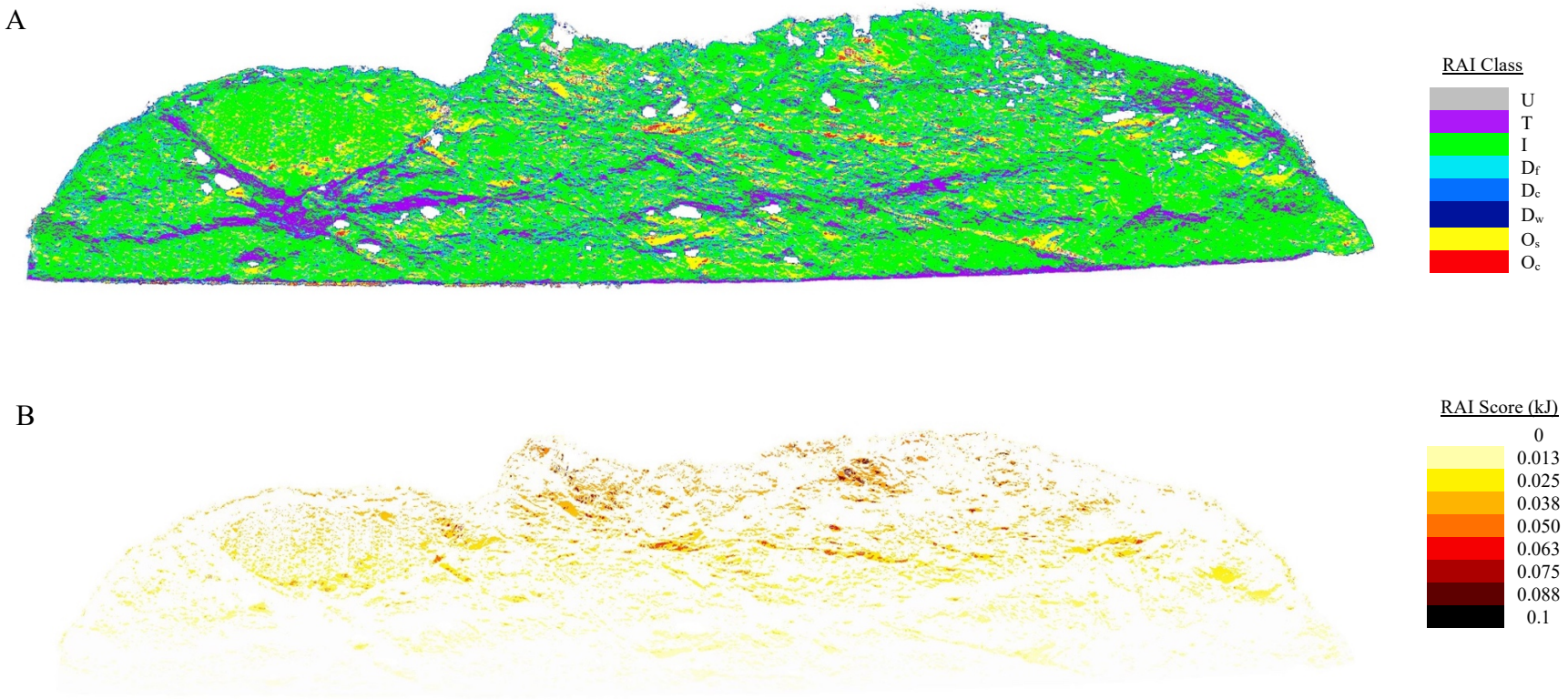

Figure 13: RAI Classes (A) and RAI Scores (B) for the 2018 scan of the study slope at MP 241 on the George Parks Highway near Glitter Gulch, Alaska. Refer to Figure 6 for a description of the RAI Classes.

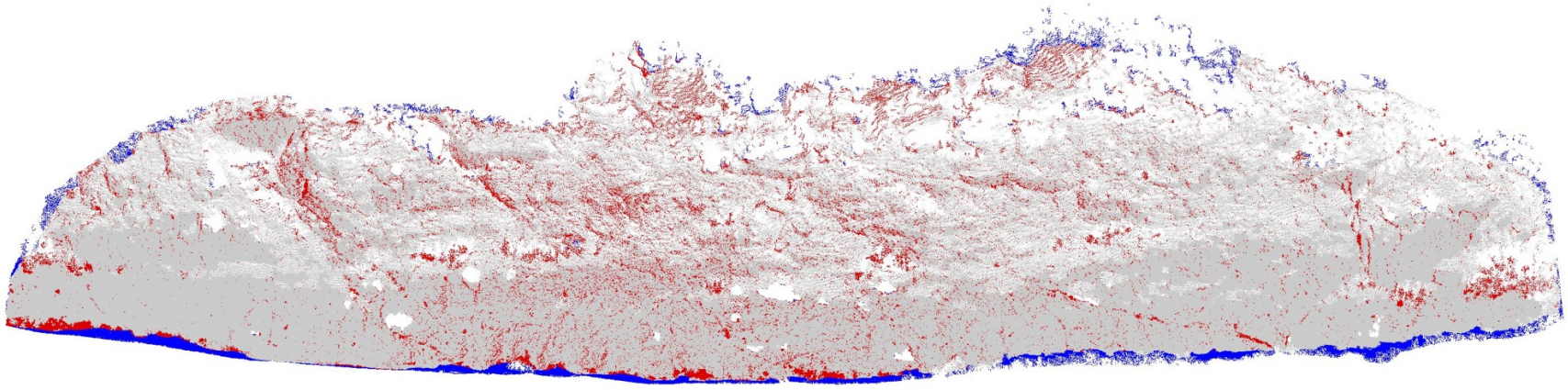

Figure 14: Change detection for Epoch 1 (2012-2013) of the study slope near MP 241 on the George Parks Highway near Denali, AK. The change from August 2012 to August 2013 is highlighted, with red representing apparent volume loss and blue representing apparent accumulation. Gains around the perimeter may represent differences in cropping of the point cloud data. The image shows the change data overlying the point cloud in grey with gradation due to changes in data density; the 2012 data was not colored RGB so an overlay with a true color image was not generated.

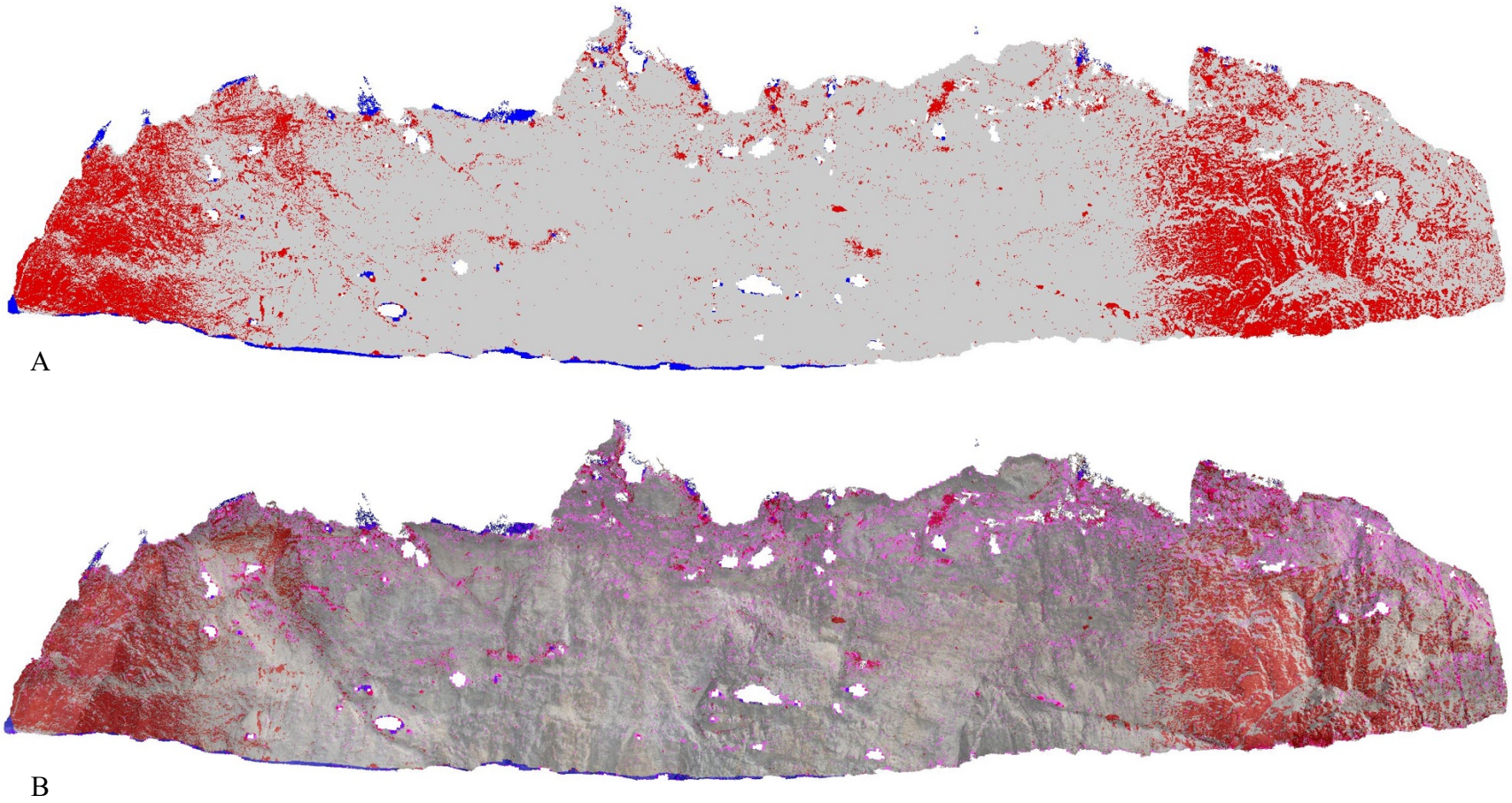

Figure 15: Change detection for Epoch 2 (2013-2014) of the study slope near MP 241 on the George Parks Highway near Denali, AK. The change from August 2013 to August 2014 is highlighted, with red representing apparent volume loss and blue representing apparent accumulation. Points created by a hole-filling algorithm are fuchsia while significant data gaps are white. Image A shows the change data overlying the point cloud in grey, while image B shows the change data overlaying a true color point cloud from 2013 data. Red areas at north and south margins of the outcrop are likely the result of misregistration of the point clouds. Gains around the perimeter of the slope may represent differences in cropping of the point cloud data.

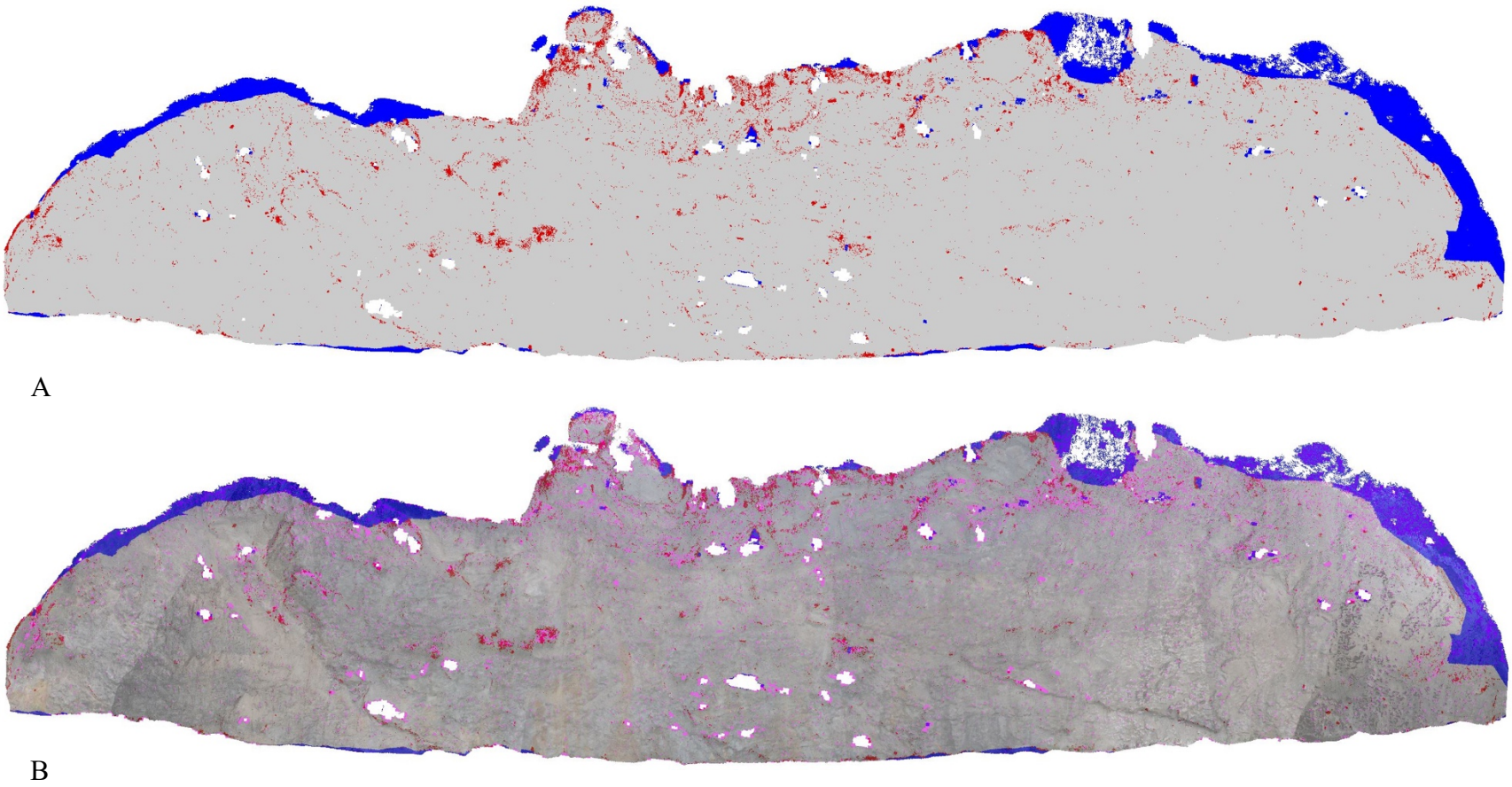

Figure 16: Change detection for Epoch 3 (2014-2015) of the study slope near MP 241 on the George Parks Highway near Denali, AK. The change from August 2014 to August 2015 is highlighted, with red representing apparent volume loss and blue representing apparent accumulation. Points created by a hole-filling algorithm are fuchsia while significant data gaps are white. Image A shows the change data overlying the point cloud in grey, while image B shows the change data overlaying a true color point cloud from 2014 data. Gains around the perimeter of the slope may represent differences in cropping of the point cloud data.

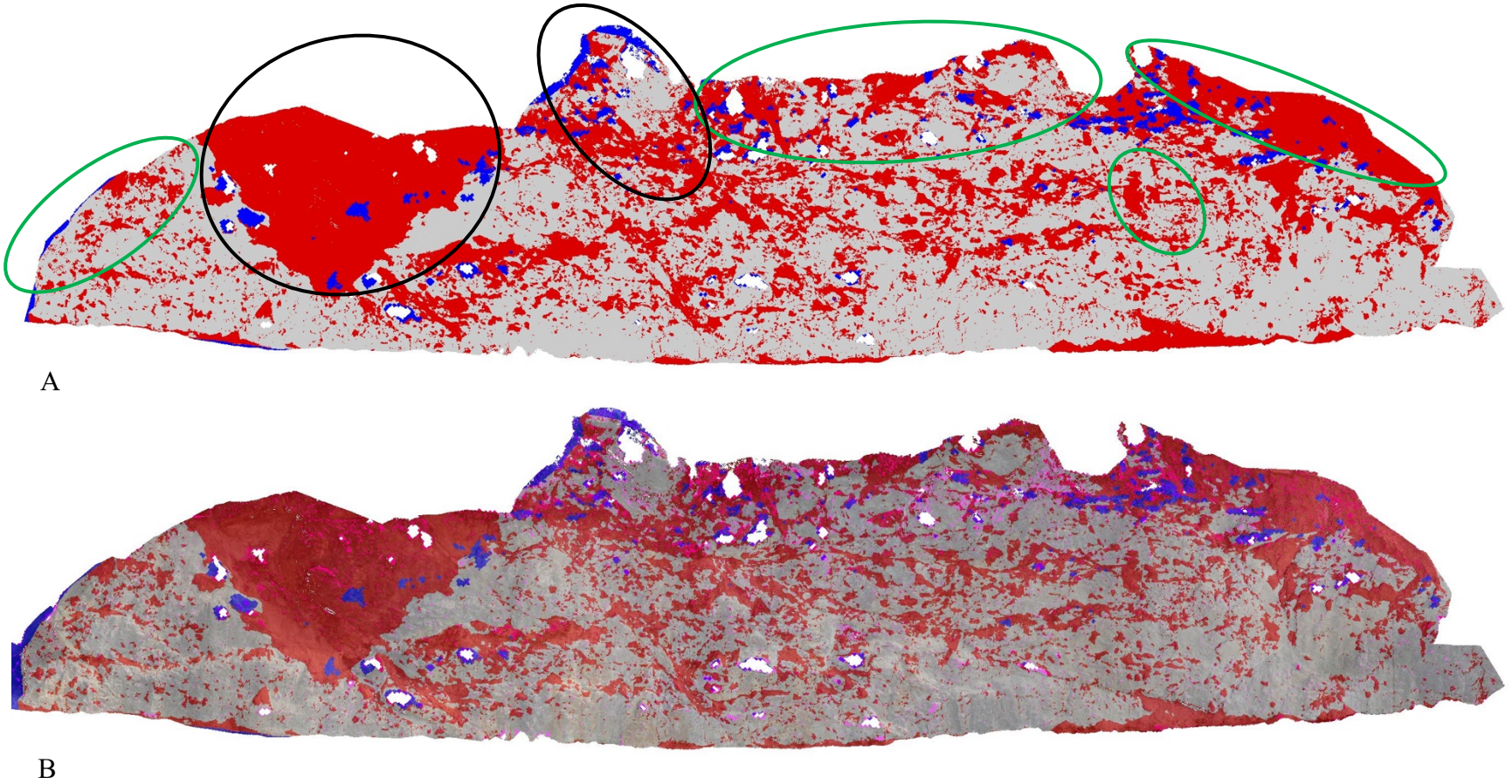

Figure 17: Change detection for Epoch 4 (2015-2017) of the study slope near MP 241 on the George Parks Highway near Denali, AK. The change from August 2015 to August 2017 is highlighted, with red representing apparent volume loss and blue representing apparent accumulation. Points created by a hole-filling algorithm are fuchsia while significant data gaps are white. Image A shows the change data overlying the point cloud in grey, while image B shows the change data overlaying a true color point cloud from 2015 data. The large change is largely a result of a 2016 slope maintenance project of scaling and trim-blasting on the slope in conjunction with re-paving of the highway. The planned areas are circled in green: scaling and black: trim blasting. Gains around the perimeter of the slope may represent differences in cropping of the annual data.

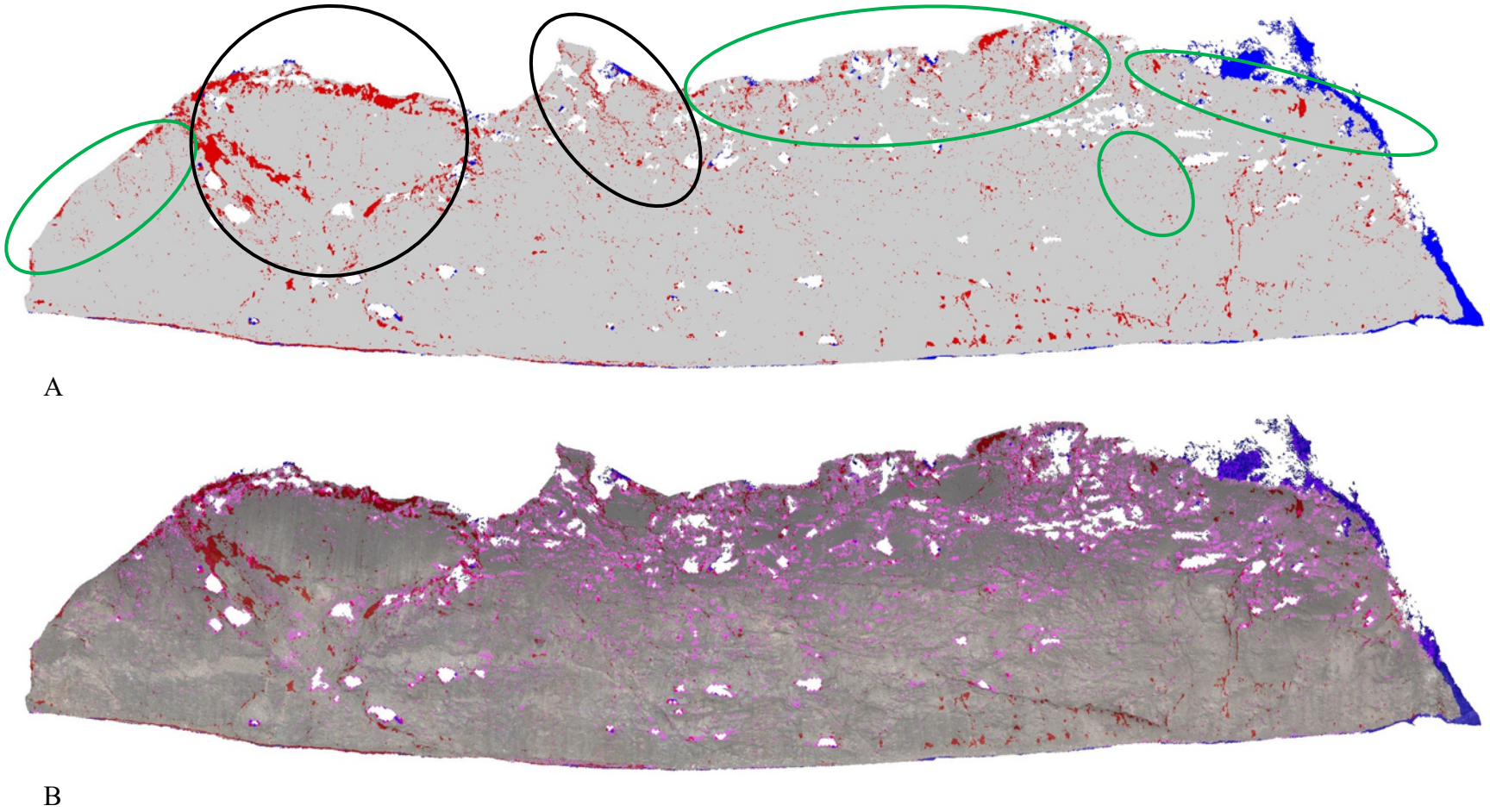

Figure 18: Change detection for Epoch 5 (2017-2018) of the study slope near MP 241 on the George Parks Highway near Denali, AK. The change data from August 2017 to August 2018 is highlighted, with red representing apparent volume loss and blue representing apparent accumulation. Points created by a hole-filling algorithm are fuchsia while significant data gaps are white. Image A shows the change data overlying the point cloud in grey, while image B shows the change data overlaying a true color point cloud from 2017 data. The planned areas for work during the 2016 scaling project are circled in green: scaling and black: trim blasting. Gains around the perimeter of the slope may represent differences in cropping of the annual data.

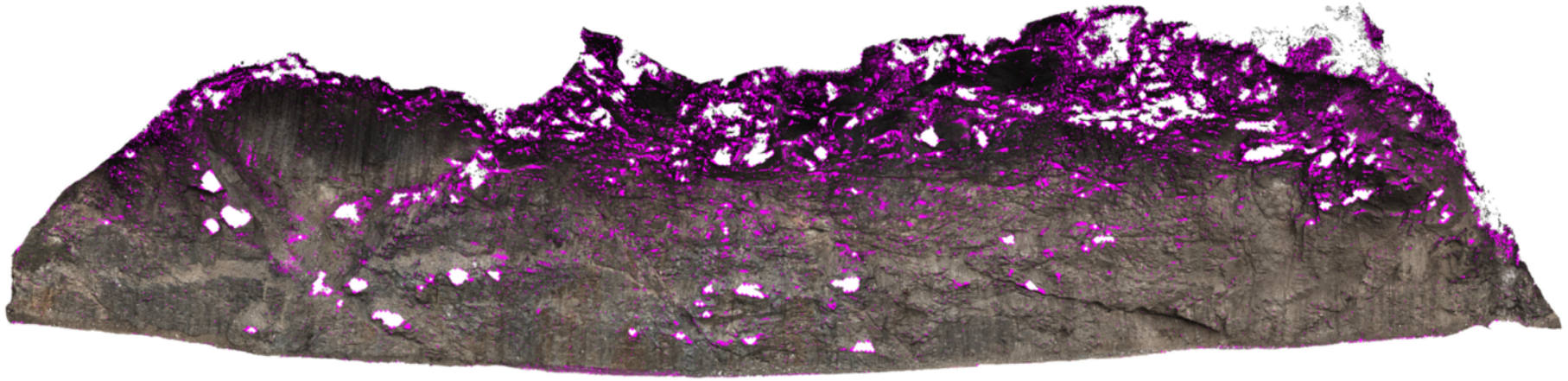

Figure 19: Point cloud of the study slope using 2018 data with hole filling outputs colored fuchsia.

Appendix: MAINTENANCE PROJECT CHANGE ORDER RELEVANT PAGES

STATE OF ALASKA
DEPARTMENT OF TRANSPORTATION
AND PUBLIC FACILITIES
NORTHERN REGION

SUPPLEMENTAL AGREEMENT NO.: 1

Sheet 1 of 2

Project No.: IM-0A4-4(15)/61275
Project Name: Parks Hwy MP 239-252 Rehabilitation

Contractor: QAP
Address: 240 W. 68th Avenue,
Anchorage, AK 99518

The above designated Contract is hereby modified in the manner described below. This agreement is supplemental to the above Contract, which is, by reference made a part hereof. Price adjustments resulting from inaccurate cost and pricing data are subject to the provisions of AS 36.30.400c. All terms, conditions, and provisions of the Contract, except as specifically modified herein, remain unchanged and in full force and effect.

Acceptance of this Supplemental Agreement constitutes agreement to the terms, conditions, and prices stated.

QAP
Contractor

Contractor Representative — Title: Construction Manager

Date: 6-1-2016

JH
Recommended: _____
Regional Construction Engineer

Issued: _____
Regional Director
For Ryan Anderson

Date: 6-2-2016

WITNESS

WHEREAS, the State of Alaska and QAP, entered into Contract No. IM-0A4-4(15)/61275 for the construction of the above referenced project, and WHEREAS the following changes in the above Contract are made in accordance with the terms of the Contract and under the terms and conditions stated below. This document shall become an amendment to the contract and all provisions of the Contract will be applicable.

1. The Standard Specifications, Standard Modifications, and Special Provisions are Modified as in Attachment #1 (12 pages).

2. Add Glitter Gulch Parks Highway Rockfall Mitigation Plans (Sheet #1-24) in Attachment #2.

3. Establish Item 203(902) Excavation and Embankment Changes- Cushioning Material, CY
   203(903) Excavation and Embankment Changes – Debris Removal, Ton
   203(904) Excavation and Embankment Changes - Weather Day Standby, CS
   203(905) Excavation and Embankment Changes- Rock Scaling – Hand Method, Scale Hour
   203(906) Excavation and Embankment Changes: Trim Blasting, LF
   640(001) Mobilization and Demobilization – SA#1 Rock Work, LS
   640(100) Workers, Meals and Lodging or Per Diem – SA#1Rock Work, Day
   641(002) Temporary Erosion, Sediment and Pollution Control – SA #1 Rock Work, CS
   643(002) Traffic Maintenance - SA #1 Rock Work, Calendar Day
   643(025) Traffic Control - SA #1 Rock Work, CS
   643(901) Traffic Control Changes – Rock Fall Barrier – SA #1 Rock Work, LF
   644(001) Field Office – SA #1 Rock Work, LS
   644(006) Vehicles - SA #1 Rock Work, LS

Use Form 25D-065 for continuation, if required

25D-066 (1/03)

STATE OF ALASKA
DEPARTMENT OF TRANSPORTATION
AND PUBLIC FACILITIES

CONTINUATION SHEET Supplemental Agreement #1, Parks Hwy MP 239-252 Rehabilitation

Project No.: IM-0A4-4(15)/61275

4. Change Amount: It is estimated that this Supplemental Agreement will alter the contract as follows:

Item No.	Description	Pay Unit	Price	Quantity	Amount
203(902)	Excavation and Embankment Changes - Cushioning Material	CY	$26.00	5,000	$130,000.00
203(903)	Excavation and Embankment Changes – Debris Removal	Ton	$18.00	75,000	$1,350,000.00
203(904)	Excavation and Embankment Changes - Weather Day Standby	CS	$200,000.00	All Req'd	$200,000.00
203(905)	Excavation and Embankment Changes - Rock Scaling – Hand Method	Scale Hour	$575.00	4,260	$2,449,500.00
203(906)	Excavation and Embankment Changes – Trim Blasting	LF	$280.00	13,345	$3,736,600.00
640(001)	Mobilization and Demobilization - SA#1 Rock Work	LS	$1,745,000.00	All Req'd	$1,745,000.00
640(100)	Workers, Meals and Lodging or Per Diem – SA#1 Rock Work	Day	$5,700.00	150	$855,000.00
641(002)	Temporary Erosion, Sediment and Pollution Control – SA #1 Rock Work	CS	$5,000.00	All Req'd	$5,000.00
643(002)	Traffic Maintenance - SA #1 Rock Work	LS	$594,000.00	All Req'd	$594,000.00
643(025)	Traffic Control - SA #1 Rock Work	CS	$1,100,000.00	All Req'd	$1,100,000.00
643(901)	Traffic Control Changes – Rock Fall Barrier - SA #1 Rock Work	LF	$250.00	2,260	$565,000.00
644(001)	Field Office – SA #1 Rock Work	LS	$113,000.00	All Req'd	$113,000.00
644(006)	Vehicles - SA #1 Rock Work	LS	$56,000.00	All Req'd	$56,000.00
			Total Amount Increased:		$12,899,100.00

5. The Contractor agrees to the following additional conditions:
   (1) Any drainage and erosion control work associated with rock work to be paid under Item 641(002) Temporary Erosion, Sediment and Pollution Control, Contingent Sum.
   (2) Item 203(904) Weather Day Standby will be paid at agreed upon $12,500.00/day rate when the weather is under one or all of the following conditions: below -5°F temperature, over 35mph wind speed, or rain event that deemed to be unsafe.
   (3) The contractor is responsible for the means to access to all work areas identified in the plans within the permitted limits. Constructing or obtaining access means is subsidiary.

6. Extend the contract time to November 3, 2016.

The Contractor certifies that, to the best of his knowledge and belief, the cost and pricing data submitted is accurate, complete, and current as of the date of execution of this Change Order and will continue to be accurate and complete during the performance of the Contract. The price to the State, including Contractor's profit or fee, will be adjusted to exclude any significant sums by which the State finds that the price is increased because the cost or pricing data furnished by the Contractor is inaccurate, incomplete, or not current as of the date of execution of this Change Order. **PLEASE INDICATE YOUR AGREEMENT BY SIGNING, DATING AND RETURNING THE ORIGINAL OF THIS DOCUMENT.**

State of Alaska
Department of Transportation and Public Facilities
NORTHERN REGION
Support Information/ Backup Sheet (Form 25D-064 - NR)

Backup for: Supplemental Agreement No. 1	Region Review J.H.
Project Number: IM-0A4-4(15) / 61275	
Project Name: Parks Highway MP 239-252 Rehabilitation	FHWA/ FAA (If required) **FHWA approved on 5/26/16**
Contract Amount: $28,866,903.50	FHWA/FAA Verbal Approval Date (If required)

COMPARISON OF COST DUE TO CHANGE

Item No.	FA Code	Item	Unit	Price	Quantity (+ or -)	*	Amount (+ or -)
203(902)	03	Excavation and Embankment Changes - Cushioning Material	CY	$26.00	5,000	*	$130,000.00
203(903)	03	Excavation and Embankment Changes – Debris Removal	Ton	$18.00	75,000	*	$1,350,000.00
203(904)	03	Excavation and Embankment Changes - Weather Day Standby	CS	$200,000.00	All Req'd	*	$200,000.00
203(905)	03	Excavation and Embankment Changes - Rock Scaling – Hand Method	Scale Hour	$575.00	4,260	*	$2,449,500.00
203(906)	03	Excavation and Embankment Changes – Trim Blasting	LF	$280.00	13,345	*	$3,736,600.00
640(001)	03	Mobilization and Demobilization - SA#1 Rock Work	LS	$1,745,000.00	All Req'd	*	$1,745,000.00
640(100)	03	Workers, Meals and Lodging or Per Diem – SA#1 Rock Work	Day	$5,700.00	150	*	$855,000.00
641(002)	03	Temporary Erosion, Sediment and Pollution Control – SA #1 Rock Work	CS	$5,000.00	All Req'd	*	$5,000.00
643(002)	03	Traffic Maintenance - SA #1 Rock Work	LS	$9,000.00	90	*	$810,000.00
643(025)	03	Traffic Control - SA #1 Rock Work	CS	$1,100,000.00	All Req'd	*	$1,100,000.00
643(901)	03	Traffic Control Changes – Rock Fall Barrier - SA #1 Rock Work	LF	$250.00	2,260	*	$565,000.00
644(001)	03	Field Office – SA #1 Rock Work	LS	$113,000.00	All Req'd	*	$113,000.00
644(006)	03	Vehicles - SA #1 Rock Work	LS	$56,000.00	All Req'd	*	$56,000.00

Prepared By: Project Manager (signature)	**Net Change This Order**	$12,899,100.00
	Total Previous Changes	$2,262,246.83
Prior Change Documents: Change Orders #1-31	**Accumulative Change**	$15,161,346.83
	% of Accumulative Change	52.52%

DESCRIPTION AND REASON FOR CHANGE

During 2015 construction, the State received a trip report for Tier II Geotechnical Assistance from FHWA Western Federal Lands, to evaluate the rockfall-prone Nenana canyon section from MP 239 to MP 241.5.

In the report, it identified 11 slopes for potentially large scale rockfall issues that cause harm to the travelling public or delays to commerce along this busy transportation route. Among them 5 slopes could fail at any time and have a

*Please encumber the amounts marked with **

Template	Object	Activity	Program	Phase	Amount
TPJ001	5012	153P	Z612750000	TC4000	$12,899,100.00

Approved: Project Manager/ Group Chief — Date: 6/1/16

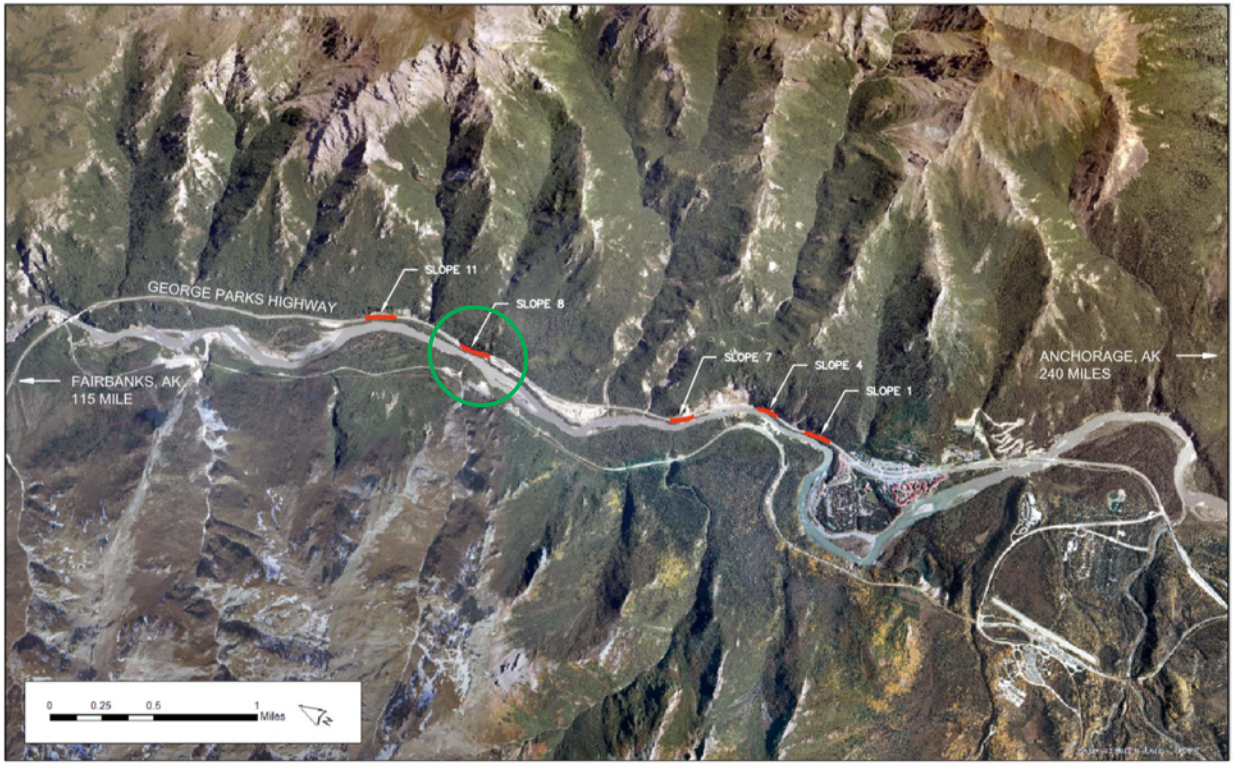

2455/AK Park Hwy - As-Built Report.dwg NAU

LANDSLIDE TECHNOLOGY
A DIVISION OF CORNFORTH CONSULTANTS
10250 S W Greenburg Road, Suite 111
Portland, Oregon 97223
Main 503-452-1200 Fax 503-452-1528

VICINITY MAP

PARKS HWY ROCKFALL - GLITTER GULCH
DENALI, ALASKA

DEC 2016
PROJ. 2455
FIG. 1